J. Phys. D: Appl. Phys. **40** (2007) R205–R228 doi:10.1088/0022-3727/40/12/R01

TOPICAL REVIEW

Organic spintronics

W J M Naber, S Faez and W G van der Wiel

SRO NanoElectronics and NanoElectronics Group, MESA+ Institute for Nanotechnology, University of Twente, PO Box 217, 7500 AE Enschede, The Netherlands

Received 12 February 2007, in final form 27 April 2007
Published 4 June 2007
Online at stacks.iop.org/JPhysD/40/R205

Abstract
We review the emerging field of organic spintronics, where organic materials are applied as a medium to transport and control spin-polarized signals. The contacts for injecting and detecting spins are formed by ferromagnetic metals, oxides, or inorganic semiconductors. First, the basic concepts of spintronics and organic electronics are addressed, and phenomena which are in particular relevant for organic spintronics are highlighted. Experiments using different organic materials, including carbon nanotubes, organic thin films, self-assembled monolayers and single molecules are then reviewed. Observed magnetoresistance points toward successful spin injection and detection, but spurious magnetoresistance effects can easily be confused with spin accumulation. A few studies report long spin relaxation times and lengths, which forms a promising basis for further research. We conclude with discussing outstanding questions and problems.

Introduction

Organic spintronics is a new and promising research field where organic materials[1] are applied to mediate or control a spin-polarized signal. It is hence a fusion of organic electronics [1–3] and spin electronics (or *spintronics*) [4–9]. Organic materials, on the one hand, open the way to cheap, low-weight, mechanically flexible, chemically interactive, and bottom-up fabricated electronics. The application of the electron's spin (instead of or in addition to its charge), on the other hand, allows for non-volatile devices, in which logic operations, storage and communication can be combined. Spintronic devices are also potentially faster and consume less electrical power [10], since the relevant energy scale for spin dynamics is considerably smaller than that for manipulating charges.

Figure 1(*a*) schematically shows the canonical example of a spintronic device, the *spin valve* (SV). Two ferromagnetic (FM) contacts with different coercive fields (H_c), applied as spin injector and spin detector, respectively, are separated by a non-magnetic (NM) spacer. The role of the spacer is to decouple the FM electrodes, while allowing spin transport from one contact to the other. The electrical resistance depends on the relative orientation of the magnetization of the two FM contacts. The relative orientation can be tuned by an external magnetic field between the antiparallel (AP) and

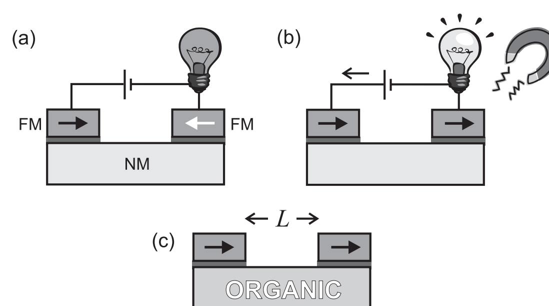

Figure 1. Schematic representation of a spin valve. Two ferromagnetic (FM) contacts (magnetization denoted by arrows) are separated by a non-magnetic (NM) spacer (bottom). One of the contacts is used as spin injector, the other one as spin detector. A tunnel barrier in between the FM contact and the NM spacer can enhance the spin signal. The light bulb schematically indicates (*a*) low conductance in the case of anti-parallel magnetization and (*b*) large conductance for parallel magnetization. (*c*) Spin valve with organic spacer with distance *L* between the contacts.

[1] The word 'organic' stems from the 19th-century belief that certain compounds, termed organic materials, could only be formed in living organisms. This belief turned out to be incorrect, but the definition is still somewhat ambiguous. Organic materials are now often defined as those materials which contain carbon–hydrogen bonds. This definition would exclude fullerenes like carbon nanotubes, as they consist of C only. Fullerenes are however mostly considered organic materials, as we also do in this review.

parallel configuration (P), as in figure 1(b). As discussed later, the resistance is usually higher for the AP configuration, an effect referred to as giant magnetoresistance (GMR)[2]. The spacer usually consists of a NM *metal*, or a thin insulating layer (in the case of a magnetic tunnel junction, MTJ). The magnetoresistance (MR) effect in the latter case is referred to as tunnel magnetoresistance (TMR). Only very recently, Lou and coworkers have demonstrated all-electric spin injection and detection using the inorganic *semiconductor* GaAs as NM spacer [12]. Semiconductor spintronics is promising, because it allows for electrical control of the spin dynamics and due to the very long spin relaxation time, multiple operations on the spins can be performed before they reach equilibrium [10].

In an organic spintronic device, the NM spacer consists of an organic material, see figure 1(*c*). The device of figure 1(*c*) is actually a *hybrid* device, since inorganic (FM contacts) and organic (NM spacer) materials are combined. In principle, also the FM contacts could be made out of organic materials (i.e. organic ferromagnets), resulting in an all-organic spintronic device. Although organic materials with FM properties do exist [13–15], to the best of our knowledge all-organic spintronic devices have not been realized so far. This review therefore focuses on structures with the hybrid geometry of figure 1(*c*).

The field of organic spintronics not only combines the aforementioned advantages of organic electronics and spintronics, it has particularly attracted attention because of the potentially very long spin relaxation times in organic materials [16]. Using electron paramagnetic resonance (EPR) measurements, room-temperature spin relaxation times in the range 10^{-7}–10^{-5} s have been found [17] (as compared with $\sim 10^{-10}$ s in metals [18]).

The spin relaxation time, τ_s, or spin lifetime, is given by

$$\frac{1}{\tau_s} = \frac{1}{\tau_{\uparrow\downarrow}} + \frac{1}{\tau_{\downarrow\uparrow}} \tag{1}$$

with the spin–flip time $\tau_{\uparrow\downarrow}$ indicating the average time for an up-spin to flip to a down-spin, and $\tau_{\downarrow\uparrow}$ for the reverse process. The spin relaxation time is a key parameter in spintronic devices, as it sets the timescale—and hence the length scale—for loss of spin polarization. The spin relaxation length, l_s, is related to the spin relaxation time as

$$l_s = \sqrt{\frac{\tau_s}{4e^2 N(E_F)\rho_N}} \tag{2}$$

in the case of a NM metal or a degenerate Fermi gas semiconductor [19, 20]. Here $N(E_F)$ is the density of states (DOS) at the Fermi level E_F, and ρ_N the resistivity of NM spacer material. For a semiconductor in the non-degenerate regime, l_s is given by [19, 20]

$$l_s = \sqrt{\frac{k_B T \tau_s}{2ne^2\rho_N}}, \tag{3}$$

[2] The qualification 'giant' is used to distinguish the effect from anisotropic magnetoresistance (AMR). AMR refers to the dependence of the electrical resistance on the angle between the direction of the electrical current and the orientation of the magnetic field [11]. The observed GMR effects are about two orders of magnitude larger.

where k_B is the Boltzmann constant, T the temperature and n the total number of carriers.

For the SV device of figure 1 to work properly, the distance L between the FM contacts should be smaller than the spin relaxation length: $L \ll l_s$. In inorganic materials, the dominant spin relaxation mechanisms are spin–orbit coupling and hyperfine interaction, which both turn out to be weak in organic materials, as discussed in section 3. The geometry of figure 1 can be used to determine l_s by varying the contact distance L and measuring the decay of the MR signal (see section 2.3.2). Such an all-electric determination of l_s is particularly interesting for organic conductors. The small spin–orbit coupling results in the absence of optical selection rules that are taken advantage of in spin relaxation measurements in (inorganic) II–VI and III–V semiconductors [21–24]. Note that (AP) FM contacts to organic light-emitting diodes (OLEDs) have been proposed to increase their emission efficiency, by increasing the relative amount of singlet excitons [25–27]. Injection of spin-polarized carriers from other FM elements like gadolinium, which is not a transition metal, into organic semiconductors has also been investigated in functional OLEDs in order to generate magnetic field dependent luminescence [28].

For the lateral GMR geometry of figure 1, it is essential that the injected spin current can be transferred over a length L with a minimum of spin relaxation. Besides the spin relaxation time, the conductivity of the organic conductor therefore needs to be sufficiently large. Whereas the long spin relaxation time is a clear advantage of organic materials, the relatively low conductivity of most organic conductors is a serious point of consideration. However, important progress has been made in recent years, see section 1. Note that in organic TMR devices the organic spacer forms a tunnel barrier, where the organic material obviously should be insulating (see section 2.2).

Another important issue in organic electronics in general, and in organic spintronics in particular, is *contacting* the organic material. Organic materials are usually fragile and the standard microfabrication techniques used for contacting inorganic materials often introduce considerable damage, making the contacts poorly defined. As spin injection and detection occurs at the interface of the FM contacts and the organic material, the quality of this interface is of crucial importance.

In this review, we present an overview of the experiments in the field of organic spintronics so far. As the field is still relatively young and rapidly expanding, this review cannot (and is not intended to) be the 'final word' on organic spintronics. Instead it is meant as a comprehensive reference for those who like to explore this new area of research. In the first part of the review, we briefly discuss the field of organic electronics (section 1), key spintronic concepts (section 2), and spin relaxation (section 3). Special attention is given to spurious MR effects that can obscure the desired spintronic characteristics and are therefore important for the correct interpretation of experimental results. In the second part, experiments on organic spintronic devices are discussed. We start with carbon nanotube experiments (section 4), followed by experiments on organic thin films of small molecules and polymers, and self-assembled monolayers (section 5). We conclude in section 6.

PART I

1. Organic electronics

Organic materials were for a long time only associated with electrical insulators. In the last century, however, the idea of organic electronics arose. On the one hand, there was the wish to use organic materials as (semi-)conductors in bulk or thin film. On the other hand, the concept was put forward to use single molecules as electrical components, such as switches and diodes. The latter field is often referred to as *single-molecule electronics* or *molecular electronics* [29]. The advantages of organic materials include chemical tuning of electronic functionality, easy structural modifications, ability of self-assembly and mechanical flexibility. These characteristics are exploited for large-area and low-cost electronic applications [30–34]. Single molecules may eventually form the ultimately miniaturized electronics, although still important issues have to be solved [2]. In this section, we briefly discuss the main developments in organic electronics.

1.1. Organic thin films

Present-day electronics is dominated by the Si/SiO_2 metal-oxide semiconductor field-effect transistor (MOSFET), where a gate voltage forms an inversion layer in between the source and drain contacts of the transistor [35]. The ability to drastically change the carrier density in semiconductors by doping and by electrical gating is essential in electronics.

Driven by the technological potential of organic materials, interest arose in organic semiconductors [36]. Present-day organic semiconductors are mainly π-conjugated materials, usually divided in *polymers* and *small molecules*, with ∼1.5–3.5 eV band gaps [37]. Thin, amorphous or polycrystalline films of these materials have been successfully applied in organic light-emitting diodes (OLEDs) [38, 39], photovoltaic cells [40, 41], and field-effect transistors (FETs) [42, 43]. Thin-film technology does not require high temperatures and lattice matching as in the case of inorganic heterostructures. Significant improvement in the performance of those devices was realized in the last few years.

Control of the carrier density by doping, as is done in inorganic (extrinsic) semiconductors, is not straightforward for most organic semiconductors as they are not pure enough. The effect of doping only manifests itself at high doping levels, since the charge states are localized due to polaronic effects (see section 1.5.3), as opposed to the delocalized states in inorganic semiconductors. As a consequence the behaviour is more metallic than semiconducting. Therefore, in organic transistors the thin-film-transistor (TFT) geometry (see figure 2(*a*)) is used rather than that of the MOSFET. In an organic TFT, a conducting channel is capacitively induced at the interface between the dielectric and the organic material. Thus the charge does not originate from dopants as in MOSFETs. Carriers are injected into the conducting channel from metallic contacts. Electrical conduction in (disordered) thin films normally results from carrier hopping between localized states (see section 1.5), and not from band-like transport through delocalized states, as typical for inorganic semiconductors.

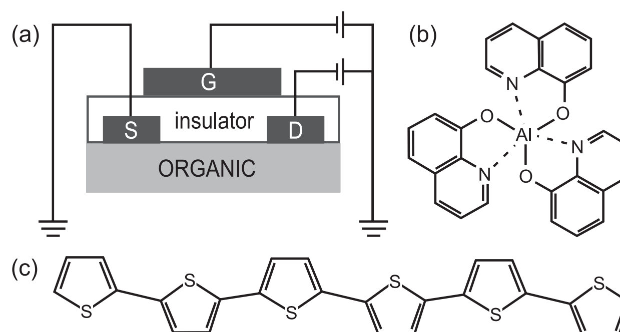

Figure 2. (*a*) Schematic layout of an organic thin-film transistor. The gate (G) electrode, which induces a conducting channel, is separated from the organic film by an insulator. The current through the organic material is injected and collected by source (S) and drain (D) contacts. Structures of two π-conjugated molecules are given: (*b*) 8-hydroxy-quinoline (Alq_3) and (*c*) the oligomer α-sexithienyl (T_6).

1.1.1. Polymers. Research on organic semiconductors first focused on improving the conductance of organic polymers. In 1963 high conductivity was reported in iodine-doped and oxidized polypyrrole [44]. Research on organic conductors was further boosted by the discovery of high conductivity in oxidized, iodine-doped polyacetylene [45, 46], for which Heeger, MacDiarmid and Shirakawa received the Nobel Prize in Chemistry in 2000. 'High conductivity' is relative in this respect, as almost all known conductive polymers are semiconductors with a low electronic mobility[3]. The maximum mobilities of polymer films are typically 0.1 $cm^2\,(V\,s)^{-1}$ [3], although there are some reports of polymers with large crystalline regions and a relative high mobility of 0.6 $cm^2\,(V\,s)^{-1}$ [47, 48]. The big advantage of polymer films though, is that there are well-developed deposition techniques available to process them.

In polymer (or plastic) electronics, especially the conjugated polymers are important [49]. These are polymers in which a sequence of alternating single and double bonds is present in the polymer chains. The wave function of one of the four valence electrons of carbon, which forms a π-bond with its neighbouring electrons, is in this case delocalized along the polymer and its mobility along one polymer chain can be rather high [50]. Next to the conduction within one molecule, also the interaction of a π-system with the π-system of a neighbouring molecule determines the conductivity of the polymer film [51]. The Peierls instability [52] causes, in practice, all conjugated polymers to act as semiconductors. The structure of polymer films is rather irregular (more or less 'spaghetti-like'), strongly limiting the carrier mobility.

1.1.2. Small molecules. More ordered films can be realized with small molecules, resulting in higher mobilities (∼1 $cm^2\,(V\,s)^{-1}$). One of the materials most commonly used for (p-type) OTFTs is pentacene with a highest reported mobility of 6 $cm^2\,(V\,s)^{-1}$ [53]. Most thin films of small molecules are grown by vapour deposition. The film-dielectric interface turns out to be of great importance for the performance of the OTFT and a lot of effort has been put in

[3] Under certain circumstances polymers can actually become metallic and even superconducting.

improving this interface, e.g. by introducing self-assembled monolayers [54]. The small organic molecule Alq_3 and the oligomer T_6, examples of organic materials that have been applied in spintronic devices, are shown in figures 2(*b*) and (*c*), respectively.

1.2. Single-crystals

Single-crystals of organic semiconductors [55] like rubrene and pentacene, are similar to the single-crystal structures of inorganic electronics. Ultra-pure organic single-crystals (OSCs) can be grown and their electronic properties are well-reproducible [33]. In OSCs grain boundaries are eliminated and the concentration of charge traps is minimized [56], making them suitable for studying the intrinsic electronic properties of organic materials and the physical limitations of organic FETs [57]. In contrast, thin films of polymers or small molecules are often strongly affected by imperfections of the film structure and by insufficient purity of the materials [58]. The electric mobilities increased largely recently, reaching room-temperature values of $35\,\mathrm{cm^2\,(V\,s)^{-1}}$ in pentacene [59] and $20\,\mathrm{cm^2\,(V\,s)^{-1}}$ in rubrene [60]. OSCs can be deposited from solution [61], but the physical vapour transport (PVT) method [3, 62] gives much better results so far. The techniques for fabricating OTFTs with as-grown OSCs has been reviewed in [33]. Recently, selective growth of OSCs on domains of octadcyltriethoxysilane was reported [63].

1.3. Single-molecule electronics

In a 1974 paper, Aviram and Ratner [64] introduced the concept of a molecular rectifier, based on the idea of 'donor-acceptor' systems already put forward in the 1940s by Mulliken and Szent-Györgi [65]. The first experimental study of single-molecule conductance was reported by Reed *et al* in 1997 [66]. One of the most important issues in single-molecule electronics is the contacting of the molecule with (metal) electrodes [67]. Obviously the contact spacing needs to be very small, typically on the order of 1 nm. The nature of the molecule-metal interface is of crucial importance to the transport properties [68]. Having good mechanical contact does not automatically imply good electrical contact. End-group engineering offers the possibility to chemically anchor the molecules to metal contacts. Apart from hooking up a single molecule to source and drain contacts, effective gating of the molecule is rather difficult due to screening of the nearby metallic contacts. Many different nanocontacting schemes have been developed over the last decade. Examples include mechanical break junctions [66], nanopores [69], electromigration [70] and conducting-probe atomic force microscopy [71].

1.4. Carbon nanotubes

Carbon nanotubes (CNTs) are carbon cylinders of a few nanometres in diameter and up to several millimetres in length [72–74]. They were discovered by Iijima in 1991 [75]. CNTs belong to the fullerene structural family, which for example also includes the C_{60} 'buckyball' molecule. They can be thought of as rolled-up graphene [76] sheets capped at their ends with hemispheres of the buckyball structure. Single-walled carbon nanotubes (SWCNTs) consist of a single carbon cylinder, whereas multi-walled carbon nanotubes (MWCNTs) are made up of multiple concentric cylinders.

The electrical properties of a SWCNT are determined by the way the graphene sheet is rolled up, expressed by the chiral vector (n, m), where the integers n and m denote the number of unit vectors along two directions in the honeycomb crystal lattice of graphene [72]. If $2n + m = 3q$ (with q an integer), the SWCNT is metallic, otherwise semiconducting. Metallic nanotubes can have an electrical current density of $1\,\mathrm{TA\,cm^{-3}}$ (i.e. $\sim$1 000 times larger than that of metals such as silver and copper) [77]. The current in MWCNTs is usually thought to mainly flow through the outermost shell [78, 79].

CNTs have attracted a lot of interest because of their exceptional electronic and mechanical properties [72]. CNTs have been applied as FETs in logic circuits [80] and have been been widely proposed for organic electronics applications [81–84]. More recently, also spin injection and transport in CNTs is intensely studied. The combination of high charge mobility, negligible spin–orbit coupling (light C atoms) and weak hyperfine interaction[4] holds the promise of very long spin relaxation lengths. The first organic spintronic device was reported by Tsukagoshi *et al* , and consisted of a MWCNT contacted by Co contacts [85].

SWCNTs have also been put forward as ideal 1D electronic systems in which Tomonaga–Luttinger-liquid (TLL) behaviour should be observable. A TLL is a model for interacting electrons (or other fermions) in a 1D conductor, where the conventional Fermi liquid model breaks down [86, 87]. The elementary excitations of the TLL are formed by separate charge and spin waves, in contrast to the quasiparticles in a Fermi liquid, which carry both spin and charge. The property that the charge and spin waves are mutually independent in a TLL is referred to as *spin-charge separation*. Spin-polarized transport in CNTs could shine more light on the electron–electron interactions in 1D systems. Balents and Egger theoretically showed that the spin-charge separation in a TLL modifies spin transport [88]. Tunnelling into a TLL is suppressed due to the strong e–e interactions in a 1D electronic system. Typical of a TLL is a power law behaviour: $\mathrm{d}I/\mathrm{d}V \sim V^{\alpha}$.

The small dimensions of CNTs also allow for the definition of a quantum dot (QD) inside the CNT. In this way, one can study the interplay of spin transport with single-charging and quantum confinement effects. In a QD also a *single* electron spin can be confined and manipulated [89]. This is particularly interesting for realizing single-spin quantum bits for quantum computing and quantum information [90].

1.5. Electronic transport in organic materials

1.5.1. Hopping versus band transport. Charge injection and transport in organic materials are still not understood in full detail. In general, one can distinguish two main charge transport mechanisms: *hopping* and *band transport*. The hopping mechanism is typical for disordered materials such as the organic thin films of section 1.1. Transport occurs via hopping between localized molecular states [91] and strongly

[4] ^{12}C has nuclear spin zero, but the isotope ^{13}C (1.1% abundancy) has nuclear spin 1/2. The concentration ^{13}C can however be reduced by isotopic purification.

depends on parameters like temperature, electric field, traps present in the material and the carrier concentration [33, 92–95]. This leads to a much smaller mobility than via delocalized band states, as in crystalline inorganic semiconductors [94]. Band-like conduction in organic materials is only expected at low temperatures for highly ordered systems [96, 97], such as the OSCs of section 1.2, when the carrier mean free path exceeds the intermolecular distance [55]. The valence band then generally originates from the overlap of the HOMO levels, and the conduction band from the overlap of the LUMO levels of the molecules [1].

1.5.2. p-type and n-type conduction. It should be noted that the terms 'n-type' and 'p-type' in organic semiconductors do not have the same meaning as for inorganic semiconductors. In the inorganic case, 'n-type' ('p-type') refers to doping with electron donors (acceptors). In the organic case, however, an 'n-type' ('p-type') material is a material in which electrons (holes) are more easily injected than holes (electrons) [3]. In organic semiconductors, p-type conduction is much more common than n-type conduction, i.e. in most organic materials hole transport is favoured. This has been explained by the fact that electrons are much more easily trapped at the organic–dielectric interface than holes [43, 98]. There are a few reports on n-type organic semiconductors [99–102], and also *ambipolar* organic materials (showing both p-type and n-type behaviour, dependent on the gate voltage) [98, 103] have been identified. However, the electron mobility is generally considerably lower than the hole mobility. For electronic logic it would be favourable to combine n- and p-type organic materials to realize complementary circuitry (as in CMOS technology [35]).

1.5.3. Polarons. As the intermolecular (van der Waals) forces in organic materials are much weaker than the covalent and ionic bonds of inorganic crystals, organic materials are less rigid than inorganic substances [104]. A propagating charge carrier is therefore able to locally distort its host material. The charge carrier combined with the accompanying deformation can be treated as a quasi-particle called a *polaron* [105]. A polaron carries spin half, whereas two nearby polarons (referred to as a *bipolaron*) are spinless [106]. Polaron formation generally reduces the carrier mobility [96, 107–112]. It is more and more realized that electronic transport in organic materials is determined not only by the characteristics of the organic conductor itself but also by the interplay with the adjacent dielectric layer [113–115]. It is therefore important to find a suitable conductor-dielectric combination [98].

1.5.4. Contacting. Apart from the conduction mechanism, the charge injection into the organic material is also of crucial importance to the performance of the device. The charge injection mechanism strongly depends on the interface between the contact and organic material. This can involve impurities, structural defects, charging, dangling bonds, dipoles, chemical moieties and other effects, in which also the fabrication method of the device plays a significant role.

Carrier injection across the metal-organic interface is determined by the energy barrier height and the density of states (DOS) at the Fermi level (E_F) of the metal contact [116, 117]. Contact resistance can be the result of a mismatch of the HOMO (for p-type semiconductors) or LUMO (for n-type semiconductors) with respect to the work function of the electrode metal. The resulting Schottky barrier gives rise to non-linear (diode-like) behaviour. The interface resistance depends exponentially on the barrier height and linearly on the DOS of the metal contact at E_F.

The Schottky barrier at the interface between a metal and organic semiconductor usually directly scales with the metal work function, as opposed to the case of inorganic semiconductors, where the Schottky barrier only weakly depends on the metal work function [37, 118]. Hence, low-work-function metals such as Ca are used to inject electrons, and high-work-function metals such as Au or InSnO (ITO) are used to inject holes into an organic semiconductor.

Since organic materials in general are rather fragile, conventional contacting methods can easily damage the material, causing a bad interface between the material and the electrode. A number of techniques have been developed for non-destructively contacting, including soft lithography (e.g. micro transfer printing) [119–121], ink-jet printing [122], solution-based methods [49, 123] and vapour phase deposition [31, 32]. The interface properties are especially important for spin injection, as is discussed in more detail in section 2.4.

1.5.5. Single-molecule transport. Transport through a single molecule is very different from bulk transport. At sufficiently low temperatures transport can be dominated by Coulomb blockade and quantum confinement effects [124–127]. In the simplest model only transport through one molecular level is considered. When this level is between the Fermi levels of the two leads, current will flow [128]. A more accurate method which is by far most used is the non-equilibrium Green's function (NEGF) method [129].

A number of methods has been developed for calculating transport [130–136]. Some of these [130–132,134], are also applicable for spin-polarized transport, e.g. in molecular SVs, consisting of a molecule sandwiched between two nanoscale FM contacts [137]. Rocha [138] shows that it is possible to obtain a very high spin-dependent signal. They used the code spin and molecular electronics in an atomically generated orbital landscape (SMEAGOL) [130]. This code combines the NEGF method with the density-functional-theory code Spanish initiative for electronic simulations with thousands of atoms (SIESTA) [139]. The code SMEAGOL is especially designed for spin-polarized transport.

Emberly and Kirczenow [140] have theoretically reproduced experiments on a gold break junction bridged with benzenedithiol molecules with a semi-empirical model. They extend this model to break junctions formed by nickel, and systems with a nickel STM tip scanning a nickel substrate covered with a bezenethiol monolayer. In both cases they find spin-valve behaviour with this model.

2. Spintronic concepts

In this section, we briefly discuss the physical mechanisms of TMR, GMR, and the conductivity mismatch problem. These concepts have been originally developed and studied for inorganic systems but are also crucial for designing and

understanding organic spintronic devices. We also discuss a number of 'spurious' MR effects that can easily be mistaken for the desired spin-valve effect.

2.1. Historical perspective

If a material or device changes its electrical resistance under the influence of an external magnetic field, this property is generally referred to as *magnetoresistance*. The first known phenomenon where the electrical resistance is altered by the direction of a magnetic moment is called anisotropic magnetoresistance (AMR), discovered in 1857 by Thomson [11]. AMR originates from the larger probability for s-d scattering of electrons in the direction of the magnetic field. The electrical resistance is maximum for current and magnetic field parallel.

In 1973, Tedrow and Meservey determined for the first time experimentally the spin polarization of the conduction band in a FM material, using a FM/tunnel barrier/superconductor junction [141]. This work led to the discovery of TMR in FM/tunnel barrier/FM junctions by Jullière in 1975 [142]. In TMR structures, the tunnelling current is proportional to the product of the DOS for each spin subband, and is hence dependent on the relative orientation of the magnetizations in both FM layers. As this relative orientation depends on the magnetic history, a TMR structure can be used as a memory [143, 144]. TMR is therefore a pure *interface effect* and does not require spin transport in the NM layer [144].

With the discovery of GMR in 1988, for the first time spin-polarized *transport* through a NM metal was demonstrated. GMR was discovered independently by Baibich *et al* [145] and Binasch *et al* [146], and triggered a tremendous amount of research on spintronic devices. The underlying mechanisms of GMR differ fundamentally from that of TMR and are discussed in more detail in section 2.3. The field of spintronics was very much stimulated by the commercial success of GMR devices. IBM already produced the first GMR-based harddisk read head in 1997 [147].

One of the long-standing goals in the spintronics community is the realization of an active device that combines electric control of the source drain current as in transistors with the memory effect of spin valves [10]. In 1990 Datta and Das proposed a FET device based on a 2D electron gas with FM contacts [148]. In the Datta-Das 'spin-FET', the current modulation between the FM contacts arises from spin precession induced by gate-controllable spin–orbit interaction. However, it was found that a strictly 1D-ballistic channel is required for this purpose [149].

The wish to combine semiconductor and spintronic concepts stimulated efforts to inject spins into a semiconductor. Using an all-optical pump-and-probe technique, Kikkawa *et al* succeeded in injecting spins in II–VI and III–V semiconductors and measuring the spin (ensemble) coherence time [21]. Very long coherence times up to 1 μs have been measured in GaAs [22–24]. The first *electrical* injection into a semiconductor was demonstrated by Fiederling *et al* [150], although the spin detection is still optical in this case. As mentioned before, only very recently an all-electrical spin injection and detection scheme was demonstrated for an inorganic semiconductor [12].

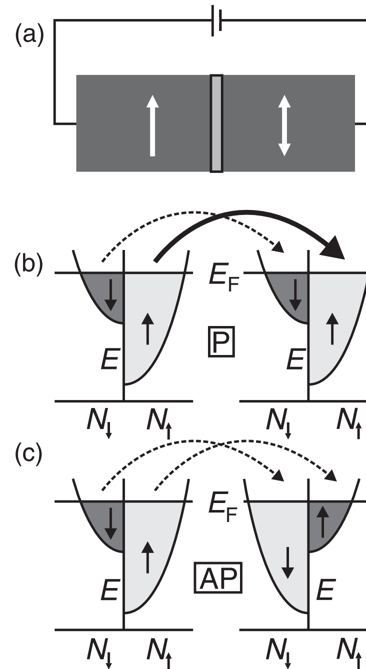

Figure 3. (*a*) Schematic representation of a TMR device, consisting of two FM materials (dark grey) separated by a tunnel barrier (light grey). The magnetization can be parallel (P) or antiparallel (AP), denoted by the arrows. Spin subbands of the FM materials are given for the P magnetization (*b*) and AP magnetization (*c*). The dashed (solid) arrow represents low (high) spin current.

One of the major obstacles for spin injection/detection in semiconductor devices is the so-called conductivity mismatch between the semiconductor spacer and the metallic FM contacts. This issue is addressed in section 2.4.

2.2. Tunnel magnetoresistance

TMR originates from the difference in the DOS at E_F between spin-up $N_\uparrow(E_F)$ and spin-down $N_\downarrow(E_F)$ electrons. Given the conservation of spin orientation during tunnelling, electrons can only tunnel from a given spin subband in the first FM contact to the *same* spin subband in the second FM contact, as schematically depicted in figure 3. The tunnel rate is proportional to the product of the corresponding spin subband DOS at E_F, and hence on the relative magnetization orientation of the contacts. Consequently, the resistance in the P configuration (figure 3(*b*)) is lower than in the AP configuration (figure 3(*c*)).

Based on the work of Tedrow and Meservey [141], assuming spin and energy conservation, Jullière derived a compact expression for the difference in resistance between the P and AP configurations, the TMR ratio[5]

$$\mathrm{TMR} \equiv \frac{R_{AP} - R_P}{R_P} = \frac{G_P - G_{AP}}{G_{AP}} = \frac{2P_1P_2}{1 - P_1P_2}, \quad (4)$$

where $R_{P(AP)}$ is the resistance in the P (AP) configuration, $G_{P(AP)}$ the conductance in the P (AP) configuration, and $P_{1(2)}$

[5] Note that the following, alternative, definitions of the TMR ratio are also frequently used:
$\mathrm{TMR}' \equiv \frac{R_{AP}-R_P}{R_{AP}} = \frac{2P_1P_2}{1+P_1P_2}$, and $\mathrm{TMR}'' \equiv 2\frac{R_{AP}-R_P}{R_{AP}+R_P} = 2P_1P_2$.

the polarization of the first (second) FM contact with

$$P_i = \frac{N_{i\uparrow}(E_F) - N_{i\downarrow}(E_F)}{N_{i\uparrow}(E_F) + N_{i\downarrow}(E_F)}, \qquad i = 1, 2. \qquad (5)$$

Although the Jullière model gives a good basic insight, it cannot explain a number of experimental observations like the dependence on temperature, bias voltage, tunnel barrier material, and the height and width of the barrier [143]. A model incorporating all these effects is still lacking.

The Jullière model treats the FM contacts as independent and is only valid for a square barrier. In real devices, the carrier wave functions from both FM contacts overlap, and a finite bias voltage gives a non-square barrier shape. Slonczewski [151] altered the Jullière model, taking into account the permeability of both barriers, resulting in an overlap of the wave functions inside the barrier. Although Slonczweski's model is more realistic, it does not account for either the temperature and voltage dependence of the TMR ratio. Vacuum tunnel barriers give MR with very little V-dependence [152]. Based on this result, two-step tunnelling through localized states in the tunnel barrier has been put forward as a possible explanation for the V- and T-dependence, as well as for negative TMR values [153–155].

Room-temperature TMR ratio's of several hundred percent have been realized [156–158], sufficiently large to make TMR hard disk read heads [159] and magnetic random access memory (MRAM) [160] commercially attractive. Since TMR relies on tunnelling through the NM layer, and not on transport as in GMR (see next section), one can apply insulating organic layers as spacer. A SAM of alkanethiols has, for example, been used for this purpose [161].

2.3. Giant magnetoresistance

The basic layout of a GMR device was already referred to in the Introduction. Analogous to the MTJ discussed above, an external magnetic field is used to switch the relative magnetic orientations of the FM layers from P to AP, or vice versa. The P configuration usually, but not necessarily, has a lower resistance. Although the working of the device seems relatively simple, the GMR effect was not predicted and its underlying principles are not straightforward. Before it was explained that TMR is *directly* related to the DOS asymmetry between the FM contacts on both sides of the tunnel barrier. Here, we will see that GMR is also related to a different DOS for both spin subbands, but in a more indirect fashion. As in the case of TMR, we assume that spin–flip scattering (i.e. the change of spin-up to spin-down, or vice versa) is negligible: $\tau_{\uparrow\downarrow}, \tau_{\downarrow\uparrow} \to \infty$. This turns out to be a very good approximation on the timescale of the dissipative processes that give rise to electrical resistivity [8]. The lack of interchange between both spin species makes it possible to treat their transport in terms of two independent transport channels, a model referred to as the *two-channel model* introduced by Mott [162–164]. We make use of this two-channel model to explain the origin of GMR in the two existing geometries described as current-in-plane (CIP) and current perpendicular to plane (CPP) (see figures 4 and 5, respectively). We assume that all conductors are in the diffusive limit, i.e. the electron mean free path is much shorter than the typical dimensions of the conductors. This assumption normally holds for organic conductors. However, in the case of CNTs transport can be ballistic, see section 1.4.

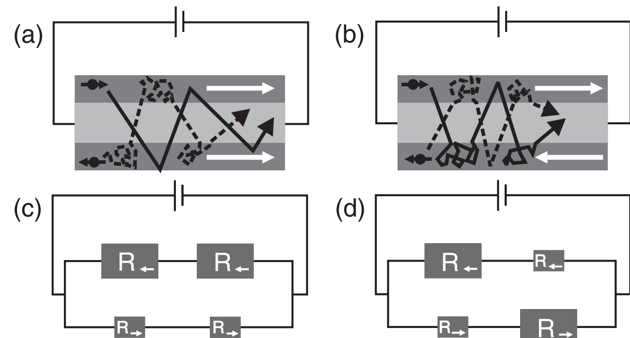

Figure 4. Schematic representation of a CIP GMR device consisting of two FM electrodes (dark grey) and a NM spacer (light grey) for the P (*a*) and AP (*b*) configuration. The magnetization is denoted by the white arrows. The trajectory of two electrons with opposite spin direction is represented by the black solid and dotted lines. The corresponding resistor model is given for the P (*c*) and AP configuration (*d*). A bigger resistor represents a larger resistance for the corresponding spin species due to enhanced scattering.

2.3.1. Current-in-plane GMR.

The first GMR devices had the CIP geometry, as they were easier to fabricate. In a FM metal, the (usually d) spin subbands are split by the exchange interaction (see figure 3), resulting in a finite magnetization at thermal equilibrium, and in a different DOS and Fermi velocity for spin-up and spin-down electrons. As a consequence, both spin species generally have different bulk conductivities, σ. In this review, we define spins oriented in the direction of the magnetization as the *majority* carriers, and spins oriented opposite to the magnetization as the *minority* carriers. The current in a FM metal is mostly carried by the electrons with the highest conductivity, normally the majority electrons, and is thus spin-polarized. The bulk current polarization α of a FM metal is defined as

$$\alpha = \frac{\sigma_\uparrow - \sigma_\downarrow}{\sigma_\uparrow + \sigma_\downarrow}. \qquad (6)$$

In a CIP GMR device (see figure 4), scattering is weak for electrons with spin parallel to the magnetization of the FM layer in which scattering takes place (they are majority carriers in this layer), whereas scattering is strong for electrons with opposite spin. Each FM layer in the CIP geometry thus favours majority carriers. When both FM layers are aligned parallel (figure 4(*a*)), the resistivity of the spin channel with spins aligned with the magnetization of both FM contacts is low (and the resistivity of the other spin channel high), resulting in an overall low resistance (figure 4(*c*)). For antiparallel alignment (figure 4(*b*)), carriers in both spin channels experience considerable scattering, resulting in an overall larger resistance ((figure 4(*d*)). The critical length scale in a CIP GMR device is the *electron mean free path*. For a sizeable effect, the NM spacer layer should be thinner than the electron mean path, and the FM layers should be thinner than the mean free path of the carriers with majority spin.

2.3.2. Current-perpendicular-to-plane GMR.

The CPP GMR geometry of figure 5 is most commonly used in organic spintronic devices. The physical origin of CPP GMR is rather different from that of CIP GMR. When a FM contact is connected to a NM material and a current is driven through the system, the spin-up current is different from the spin-down

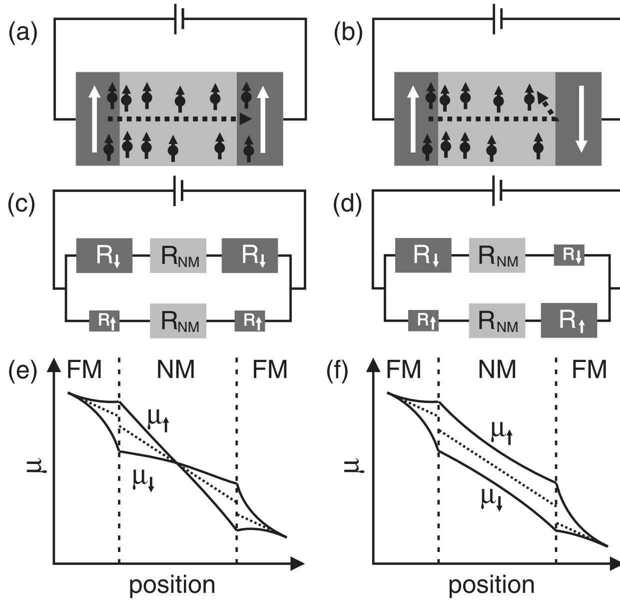

Figure 5. Schematic representation of a CPP GMR device consisting of two FM electrodes (dark grey) separated by a spacer (light grey) for the P (*a*) and AP configuration (*b*). The magnetization of the FM electrodes is denoted by the white arrows. The dotted arrows represent the spin current. The corresponding resistor model is given for the P (*c*) and AP configuration (*d*). The colours correspond to the layers in (*a*) and (*b*), and bigger resistors represent a larger resistance for the denoted spin species. The electrochemical potentials μ for the two spin species are given for the P (*e*) and AP configuration (*f*). The dotted lines are the asymptotes of the electrochemical potentials to which they would collapse at large distances. The dashed lines correspond to the interfaces in (*a*) and (*b*).

current, due to the current polarization in the FM. A finite magnetization builds up in the NM material, which is known as *spin accumulation* [165]. The spin accumulation is defined as the difference between the electrochemical potential for spin-up electrons, $\mu_\uparrow$, and that for spin-down electrons, $\mu_\downarrow$. The magnitude of the spin accumulation depends on the spin injection rate into the normal material and the spin relaxation time, and it decays exponentially away from the injecting contact on a length scale set by the spin relaxation length

$$\mu_\uparrow - \mu_\downarrow \propto \exp(-l/l_s), \tag{7}$$

where l is the distance from the injecting contact. The net spin density resulting from the spin accumulation is typically orders of magnitude smaller than the charge density in the NM. However, the spin accumulation in the NM can be probed by a second FM contact, the spin detector, if it is placed at a distance smaller or comparable to the spin relaxation length from the spin injector.

A finite spin accumulation implies different densities of spin-up and spin-down carriers at the site of the detector interface. The transmission is now largest when the magnetization of the detector contact is parallel to the net spin accumulated at its interface. CPP GMR can also be described in terms of a parallel resistor model, as shown in figures 5(*c*) and (*d*). A more thorough theoretical description of CPP GMR based on the Boltzmann equation has been provided by Valet and Fert, for which we refer to [166]. With their model, the electrochemical potentials of the two spin species can be calculated, as illustrated in figures 5(*e*) and (*f*). It reveals the splitting of the electrochemical potentials at the interfaces of the FM contacts and NM material. It also shows the different voltage drop (represented by the discontinuity of the asymptote) at the interfaces for the P and AP configuration, which leads to the difference in resistance between these two cases. It is important to note that the critical length scale for CPP GMR devices is the *spin relaxation length*, and not the electron mean free path, as for CIP GMR. As the spin accumulation decays exponentially from the injector, the GMR ratio depends exponentially on the distance between injector and detector. This feature is very useful for determining the spin relaxation length in (organic) materials.

Besides the basic trilayer CIP and CPP geometries described above, GMR has been observed in multilayer systems [145], granular systems [167] and nanocontacts [18].

2.4. Conductivity mismatch problem

A fundamental obstacle for spin injection from a FM metal into a semiconductor is the so-called *conductivity mismatch problem* [19, 168–173]. The conductivity of a semiconductor is usually much lower than that of a metal. In a SV, one likes to detect the resistance change due to the different magnetization orientations in the FM layers. If the resistance of the whole device is dominated by the resistance of the semiconductor spacer, the overall resistance change is negligible. This can also be seen from the resistor model in figure 5. When the resistance of the NM material, R_{NM}, is much larger than the other resistances, this dominates the overall resistance and no change is observed. This is particularly relevant for organic spintronics, since most organic materials are much less conductive than the FM contacts.

There are two possible solutions to this problem. The first one is to use a fully spin-polarized FM material, i.e. a *half-metal* such as $LaSrMnO_3$ (LSMO) [70, 174]. In the classical FM materials (e.g. Fe, Ni, Co), the conduction electrons mainly have 4s character, whereas the polarized electrons are in the, more localized, 3d-band. This electronic structure leads to a spin polarization at the Fermi level far below 100%: Co is the best elemental ferromagnet with $P = 45\%$ [175]. In a half-metal, only one spin subband is occupied at the Fermi level and the spin polarization P therefore approaches 100% at low temperatures. In the case of LSMO ($T_C \sim 370$ K), there is a fully polarized conduction band of 3d character at E_F and no s band. Even if the bulk properties of a material indicate half-metallic behaviour, it is not *a priori* clear, however, whether the spin polarization can efficiently be transferred across the interface with a NM material. The maximum contact spin polarization value observed in MTJs with LSMO is 0.95 [174]. LSMO contacts have been applied in SV devices with CNTs and organic thin films (see sections 4 and 5, respectively).

Another possible solution for the conductivity mismatch problem is the introduction of a large spin-dependent resistance [19, 171–173]. This spin-dependent resistance could be a tunnel barrier in between the FM contact and semiconductor spacer. This spin-dependent resistance gives a larger change in resistance between the P and AP configuration, as can be visualized by the resistor models in figures 6(*c*) and (*d*). In the

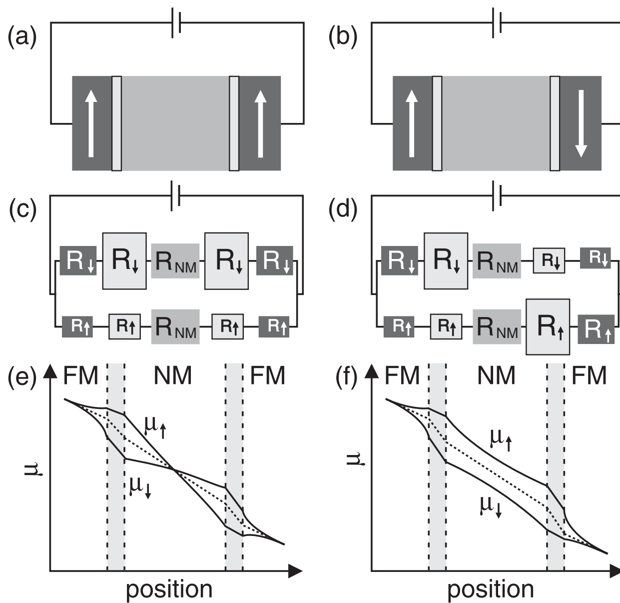

Figure 6. Schematic representation of a CPP GMR device consisting of two FM electrodes (dark grey) separated by a spacer (light grey) and tunnel barriers (light grey with black outline) for the P (*a*) and AP configuration (*b*). The corresponding resistor model is given for the P (*c*) and AP configuration (*d*). The shading corresponds to the different parts in (*a*) and (*b*). The electrochemical potentials μ for the different spin species are given for the P (*e*) and AP configuration (*f*). The dotted lines are the asymptotes of the electrochemical potentials to which they would collapse at large distances. The dashed lines correspond to the interfaces in (*a*) and (*b*).

model by Valet and Fert this will lead to a larger spin splitting at the interface and a larger difference in the voltage drop over the whole device for the two configurations (see also figures 6(*e*) and (*f*)).

In the case of organic spacers, next to the bulk conductivities of the FM contacts and the organic material and the interface resistances, also the ratio of polarons to bipolarons is of importance. Bipolarons have no spin and the spin-polarized current is only carried by polarons. Ren *et al* [176] find, like in the case of inorganic semiconductors, an increase of the spin polarization when the conductivity of the organic material approaches or surpasses the conductivity of the FM material and when a spin-dependent interface resistance is introduced. The influence of the bipolarons is not drastic. When there are only bipolarons the spin polarization is zero of course, but when the fraction of polarons is only 20%, the spin polarization is 90% of the value attainable with only polarons and no bipolarons.

2.5. Spurious effects

Injecting and detecting spins in a NM material is not trivial, as is apparent from the discussion of the conductivity mismatch problem above. In this section, we discuss a number of phenomena (or 'spurious effects') that can give rise to MR effects, but are not related to (but are easily mistaken for) the TMR and GMR effects described above. For the correct interpretation of organic spintronic experiments, it is crucial to take these effects into account.

The Lorentz force curves the electron trajectories and has a (positive) MR effect on the order of $(l_e/l_B)^4$, where $l_B = \sqrt{h/(eB)}$ is the magnetic length [177]. Lorentz magnetoresistance (LMR) is relevant for systems with a relatively large mean free path, such that $\omega_c\tau > 1$, where ω_c is the cyclotron frequency and τ the elastic scattering time [178]. In systems where transport takes place by hopping, a magnetic field can enhance the localization of the carriers on the hopping sites, thereby also increasing the resistance [179].

In the coherent, diffusive transport regime, conductance can be affected by a magnetic field via electron interference phenomena such as weak localization (WL) and universal conductance fluctuations (UCF) [180]. WL is interpreted as coherent backscattering and gives rise to an enhanced resistance around $B = 0$, where the width of the resistance maximum is determined by the (charge) coherence length, l_ϕ. UCF are of the order e^2/h, regardless of the sample size and the degree of disorder (hence the name 'universal'). UCF result from the microscopic change in electron interference paths due to a change in E_F, impurity configuration or enclosed magnetic flux.

Another MR effect that is not caused by spin accumulation in the NM material is the *local Hall effect*. Stray fields coming from the FM contacts can penetrate the NM spacer and induce local Hall voltages. When the magnetization of the FM contacts changes, so do the Hall voltages [181, 182]. In this way, these voltages can obscure the true SV signal.

In small systems, such as CNTs, where Coulomb charging effects are relevant, the *magneto-Coulomb effect* (MCE) can play a role [183]. Due to this effect, the conductance in a system connected to two FM leads changes as a function of magnetic field, but not due to spin accumulation. In a FM contact, the spin subbands are shifted by the Zeeman energy in the opposite direction under the influence of an external magnetic field. As the DOS at E_F in a ferromagnet is in general different for both spin species, repopulation of the electrons takes place through spin–flip scattering. This gives a shift in the chemical potential [184]. When the FM contacts are connected to large NM leads, the change in chemical potential in the FM contacts causes electrons to flow across the FM/NM interface. This leads to a change in the dipole layer at the interface. The voltage change can couple to the conductor in between the two FM leads via the capacitance and therefore effectively acts like a gate. As the magnetization of the FM material switches its direction at the coercive field, the conductance changes discontinuously at this field due to the MCE. The MCE can therefore easily be mistaken for the SV effect in small structures [183].

In principle, it is possible to calculate the magnitude of the above spurious effects or measure them in control devices [185]. However, a more elegant and rigorous way to rule out the discussed effects is to measure spin accumulation using the so-called *non-local geometry* of figure 7 [18, 165]. A current is injected by two contacts, while the voltage is measured by two other contacts. When at least two contacts are FM, the spin accumulation can be probed in such a way that the measured spin diffusion is isolated from the current path. In this way, the measured signal is only due to spin accumulation.

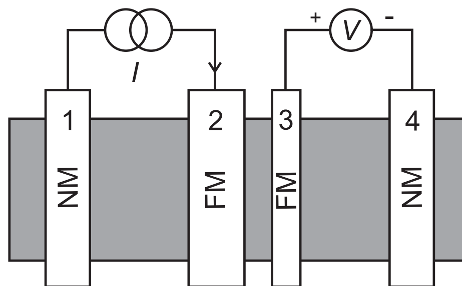

Figure 7. Non-local geometry for measuring spin accumulation. A current is driven between electrodes 1 and 2, while the voltage is measured between electrodes 3 and 4. When electrode 2 is FM, a spin-polarized current is injected. The spins diffuse in both directions and can thus be probed by electrode 3, which is also FM. Therefore a voltage difference is observed between the parallel and antiparallel states of the two FM electrodes. As the measured voltage is not influenced by the charge current, the signal is purely due to spin accumulation.

3. Spin relaxation

In general, one can distinguish two classes of spin relaxation. The first one describes the decay of a net spin component along the axis of spin quantization, which we define as the z-axis. The z-component (or *longitudinal* component) of the total spin, S_z, decays exponentially to equilibrium due to individual spin–flips on a timescale T_1. This T_1 is equal to the spin relaxation time τ_s, defined in (1). As this process requires energy exchange with the environment, it is a rather slow process. There is a second process, however, that does not require energy exchange and affects the spin component perpendicular to the quantization axis, i.e. the *transverse* component $S_\perp$. This process affects the quantum-mechanical phase of individual spins and leads to loss of *coherence* on a timescale T_2. For different spins within an ensemble the phases are in general affected unequally, which results in the spins getting out of phase. The timescale related to this process of ensemble dephasing is often denoted as T_2^* [186–188]. Usually $T_2^* < T_2$, an effect referred to as *inhomogeneous broadening*. The time evolution of a spin ensemble with total spin[6] $\boldsymbol{S}$ in an external magnetic field $\boldsymbol{B}$ along the z-axis can then be described by the Bloch equations

$$\frac{\mathrm{d}S_z}{\mathrm{d}t} = \gamma(\boldsymbol{B}\times\mathbf{S})_z - (S - S_z)/T_1 \qquad (8)$$

$$\frac{\mathrm{d}S_\perp}{\mathrm{d}t} = \gamma(\boldsymbol{B}\times\mathbf{S})_\perp - (S - S_\perp)/T_2^*, \qquad (9)$$

where γ is the gyromagnetic ratio.

In this section, we discuss the underlying mechanisms for spin relaxation in solids, divided in mechanisms related to spin–orbit coupling and to hyperfine interaction. Both spin–orbit coupling and hyperfine interaction are expected to be small, but not completely negligible for most organic materials. The dominant relaxation mechanisms in organic materials are still rather unclear. There are a few reports where the spin relaxation length is determined from fitting to Jullière's formula, but it is hard to distinguish between spin relaxation at the interfaces and within the organic material itself. Also, the simple Jullière formula (4) is not always very appropriate for the applied device configurations.

[6] We use the symbol $\boldsymbol{S}$ for the resultant spin vector of a spin ensemble, whereas $\vec{S}$ is used for denoting an individual spin vector.

3.1. Spin–orbit coupling

Spin–orbit coupling is a relativistic effect, describing the interaction between the electron's spin and its orbital motion around an atomic nucleus. More generally, spin–orbit coupling occurs whenever a particle with non-zero spin moves in a region with a finite electric field. In the rest frame of a particle moving at a relativistic velocity, a static electric field Lorentz-transforms in a field with a finite magnetic component. Thus, although the spin degree of freedom only couples to a magnetic field, it is indirectly affected by an electric field via spin–orbit coupling. The electrical field can have various physical origins, such as the electric field of an atomic nucleus or the band structure of a solid [144].

As spin–orbit coupling generally grows with atomic number Z (it scales as Z^4 in the case of an hydrogen-like atom [16]), and organic materials consist mainly of low-Z materials (in particular C), spin–orbit coupling is usually small in organic materials. Sulphur atoms could provide a considerable spin–orbit coupling, but these atoms normally play a marginal role in carrier transport in organic materials [189]. Depending on the exact band structure of the organic material, spin–orbit coupling is actually not always negligible [190].

In (inorganic) solids one can distinguish two main contributions to spin–orbit coupling. The first one, termed the *Dresselhaus contribution*, occurs in crystals that exhibit bulk inversion asymmetry, which implies that there is a net electric field for certain crystal directions [191, 192]. The second one, referred to as the *Rashba contribution*, occurs in systems with net electric fields due to structural inversion asymmetry [171, 193]. Three different spin–orbit-coupling-related spin relaxation mechanisms can be distinguished in non-magnetic solids: Elliot–Yafet (EY), D'yakonov–Perel (DP), and Bir–Aronov–Pikus (BAP).

The EY mechanism [194] is due to the fact that under the influence of spin–orbit coupling momentum eigenstates are no spin eigenstates anymore. Any momentum scattering event has hence a finite probability to flip the spin. The EY mechanism leads to a spin relaxation time τ_s that is proportional to the momentum scattering time. Momentum scattering is mainly caused by impurities at low temperature and phonons at high temperature [9]. Usually EY is the dominant mechanism in metals, and it has recently been claimed to be dominant in organic semiconductors as well [195, 196].

The DP [192] mechanism arises when the solid lacks a centre of symmetry and is therefore directly related to the Dresselhaus contribution. As the internal magnetic field is $\vec{k}$-dependent, the axis around which the spin precesses is randomized upon electron (momentum) scattering. This results in a loss of memory of the initial spin direction. Heavy scattering slows down the spin relaxation because the spin cannot follow the internal magnetic field when it changes too rapidly. Therefore, the spin relaxation time is inversely proportional to the scattering time.

The BAP [197] mechanism is caused by electron–hole exchange interaction, and therefore only plays a role in systems

where there is a large overlap between the electron and hole wave functions.

The spin–orbit-coupling-related relaxation mechanisms directly affect T_1, and indirectly T_2.

3.2. Hyperfine interaction

Another source for spin relaxation is the hyperfine interaction. It originates from the interaction of the electron spin with the nuclear spins of the host material. In general, the electron spin interacts with many, say N, nuclear spins. The electron–nuclear coupling Hamiltonian is then given by

$$H_{\mathrm{hyp}} = \sum_{i}^{N} A_i \vec{I_i} \cdot \vec{S}, \tag{10}$$

where $\vec{I_i}$ and $\vec{S}$ are the spin operator for nucleus i and the electron spin, respectively, and A_i the coupling strength between them.

The nuclear spins affect the spin relaxation time T_1 by means of so-called electron-nuclear flip-flops. In addition, fluctuating nuclear spins also result in dephasing, thus affecting T_2. For an electron spin interacting with N nuclear spins, the statistical fluctuation scales with $\frac{1}{\sqrt{N}}$ [198, 199]. Hence the more delocalized the electron wave function is, the less the influence of the nuclei.

The nuclear spins in organic materials are mainly originating from the isotopes ^{1}H ($I = 1/2$), ^{13}C ($I = 1/2$), and ^{14}N ($I = 2$). Despite the presence of nuclear spins, the hyperfine interaction in organic materials is usually weak. The reason is that for organic conductors often use is made of π-conjugated molecules with delocalized states (see section 1) that have practically no overlap with the C or H atoms, since the wavefunctions of the π-electrons mainly consist of p_z orbitals, whose nodal plane coincides with the molecular plane [16].

PART II

4. Carbon nanotube devices

In this section, we discuss experiments on organic spin valves where the spacer between the FM electrodes is formed by a CNT, including tunnelling or diffusive junctions. Generally, the CNT is considered to be a quasi-spin-ballistic waveguide. Where purely metallic systems (such as the GMR multilayer systems discussed in section 2.3.2) have the advantage of large carrier velocity, τ_s is very short ($\sim 10^{-10}$ s). (Organic) semiconductors, on the contrary, have much larger τ_s (up to $\sim 10^{-6}$ s), but the carrier velocities are smaller. CNTs combine a high carrier velocity ($\sim 10^6$ m s^{-1}) with a potentially very long τ_s. Electronic transport can also occur in different regimes, depending on the transparency of the contacts. High contact resistance leads to quantum-dot behaviour, while transparent contacts give transport determined by quantum interference [200]. It is therefore no surprise that the field of organic spintronics took off with work on CNTs and that there is still a lot of activity going on.

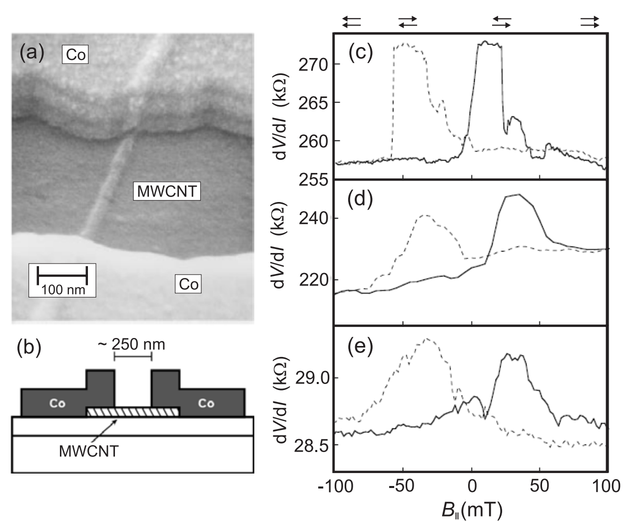

Figure 8. (*a*) Scanning electron microscope picture and (*b*) schematic diagram of a device, consisting of a MWCNT connected by two 65 nm thick polycrystalline Co contacts, fabricated by EB lithography and thermal evaporation. The contacts lie on top of the MWCNT and are separated by 250 nm. The diameter of the MWCNT is 30 nm (diameters range from 10–40 nm) and the length more than 1 μm. NM leads are deposited more than 30 μm away from the MWCNT. The device is fabricated on a semi-insulating Si wafer covered by 200 nm SiO_2. The two-terminal differential resistances of three different MWCNT devices at 4.2 K are given in (*c*), (*d*) and (*e*). The magnetic field is parallel to the substrate and the obtained MR values are (*c*) 6%, (*d*) 9% and (*e*) 2%. The arrows at the top of the graph denote the magnetization of the left and right contact. Courtesy of Tsukagoshi *et al* [85].

4.1. Multi-wall carbon nanotubes

The first organic spintronic device ever was realized by Tsukagoshi and coworkers [85]. It consisted of a single MWCNT contacted by polycrystalline Co contacts, see figure 8(*a*). The device layout is schematically given in figure 8(*b*). The MWCNTs were synthesized by the arc discharge evaporation method in a He atmosphere to avoid contamination by magnetic impurities (e.g. from catalyst particles). The Co top contacts are defined by electron-beam (EB) lithography and thermal evaporation.

Examples of MR measurements at 4.2 K are given in figures 8(*c*)– (*e*). There is a rather large sample-to-sample variation in the differential resistance, most probably due to irreproducible contact resistances. CoO could for example be formed at the interface. Residues from the resist layer cannot be excluded either. A hysteretic resistance increase of $\sim$50 mT width is observed around $B = 0$, suggesting spin-valve behaviour. The two Co contacts are nominally the same and should therefore have the same coercive field. The authors nevertheless argue that AP alignment is possible due to local magnetization fluctuations on the scale of the MWCNT diameter (30 nm). A maximum 9% MR (MR $\equiv (R_{\mathrm{AP}} - R_{\mathrm{P}})/R_{\mathrm{P}} \approx (R_{\mathrm{AP}} - R_{\mathrm{P}})/R_{\mathrm{AP}}$) is reported for these devices at $T = 4.2$ K. The MR decreases approximately exponentially with T and disappears around 20 K. The T-dependence is ascribed to the poor quality of the MWCNT/FM interface. In later reports, on the same device structure [201, 202], it was observed that the MR becomes negative above 20 K before

completely disappearing at 175 K. The negative MR is possibly due to the presence of CoO [202] or due to the negative spin polarization of the Co d-band, where the majority spin DOS at the Fermi level is smaller than the minority spin DOS.

Comparing with a simple approximation based on the Jullière model and neglecting the influence of the MWCNT-Co interfaces, Tsukagoshi *et al* find $l_s \sim 130$ nm [85]. As this estimate is based on only one distance between the FM contacts (250 nm), it does not take into account spin relaxation at the interfaces. The estimate is therefore likely to be a conservative one. Stray magnetic fields from the FM contacts can affect the resistance of the MWCNT by suppressing weak localization (see section 2.5). For this experiment the difference in stray fields between the AP and P configuration is estimated to be responsible for a maximum MR of 0.3% [203], hence smaller than the observed maximum of 9% in [85]. For comparison, devices of the same geometry but with one FM (Co) contact and one NM contact (Pt/Au) were also measured, showing no hysteretic MR contrary to the former devices [203].

Similar devices have been tested again by this group [202] and other groups [204–207]. Although MR behaviour has been repeatedly reported, there is a major lack of consistency both qualitatively and quantitatively.

An alternative contacting method, involving shadow mask evaporation was introduced by Orgassa *et al* [204]. They used a 4 μm tungsten wire as a shadow mask over an orthogonally placed NT and evaporated Co and NiFe electrodes from two different angles, resulting in a 1 μm contact spacing. A maximum 2.2% negative and 0.6% positive MR was reported in two out of ten Co/MWCNT/NiFe devices below 30 K. Comparing the MR results with the Jullière model and using contact spin polarizations taken from the literature, gives 380 nm as the lower limit for the spin relaxation length in the MWCNT. Similar to Tsukagoshi *et al*, this estimate is only based on one contact spacing and therefore does not account for spin relaxation due to interface imperfections. It is likely that also in this experiment the growth conditions of the electrodes dominate the device performance. Orgassa *et al* have also proposed a concept for spin-resolved scanning tunnelling microscopy (SR-STM), based on a CNT acting as the tunnelling tip in proximity to a magnetic sample (see figure 9) [204].

A very large increase in MR was reported by Zhao *et al*, claiming 30% [205] and −36% [206] MR in Co/MWCNT/Co devices at small bias currents at 4.2 K. Their fabrication method is very much like Tsukagoshi's and a wide range of device resistances is reported here as well. The MR signal decreases with bias current and disappears above 10 K. At low temperature non-linear transport is observed, possibly caused by Coulomb blockade in the ∼200 nm long devices.

Considerable improvement in realizing reliable, low-ohmic contact resistance was achieved by the introduction of $Pd_{0.3}Ni_{0.7}$ electrodes by Sahoo *et al* [208]. The contact resistance can be as low as 5.6 kΩ at 300 K. While the Pd alloy is expected to have the same contact properties—such as low-resistance and quasi-adiabatic contacts—as pure Pd contacts to CNTs [209], the high Ni concentration provides the required spin current. The spin polarization in $Pd_{0.3}Ni_{0.7}$ is estimated at 9.58%, and the $Pd_{0.3}Ni_{0.7}$ thin-film Curie temperature and saturation magnetization are half the bulk values [208]. This

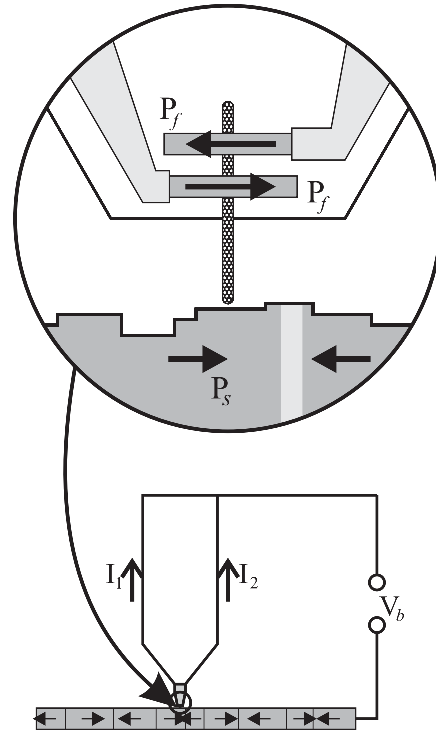

Figure 9. Setup for spin-resolved scanning tunnelling microscopy with a CNT tip, as proposed by Orgassa *et al* . The spin polarization in the contacts P_f determines the asymmetry in the currents $I_{1,2}$. Reprinted from [204] courtesy of Orgassa *et al*.

is ascribed to partial oxidation of the Ni during evaporation. A low device resistance, and in particular a low contact resistance, is not required *a priori* in a spintronic device, as was pointed out in section 2.4. However, low contact resistance avoids charging effects and hence the magneto-Coulomb effect, see section 2.5. A maximum MR value of ∼2% is reported at 1.8 K and 2 V back gate voltage. The MR is however strongly dependent on the gate voltage and disappears at zero gate voltage, which was not understood.

The gate-voltage dependence of the MR was worked out in more detail in an experiment by the same group [210], where the MR magnitude and sign could be gate-field-tuned in a predictable way, see figures 10(*a*)–(*c*). The MR varies here almost regularly between −5% and +6% on a gate-voltage scale of ∼0.5 V at 1.85 K. The MR oscillation cannot be explained in terms of Rashba spin–orbit coupling [193], as proposed by Datta and Das [128], since the spin–orbit coupling is too low in CNTs (see section 3.1). Alternatively, the oscillatory behaviour was shown to be consistent with quantum interference as predicted originally for semiconductor heterostructures [211]. As was shown in measurements at lower temperature ($T = 300$ mK), the MWCNT behaves as a quantum dot [124, 125]. Weak disorder in the MWCNT causes the single-electron resonances to be modulated in amplitude, see figure 10(*b*). The MR signal (figure 10(*c*)) is claimed to follow this envelope function, which is substantiated in the discussion of their SWCNT experiment in section 4.2.

In the experiments discussed so far, metallic FM contacts were attached to the MWCNTs. Hueso *et al* [212] instead applied single-crystal $La_{2/3}Sr_{1/3}MnO_3$ (LSMO), which is

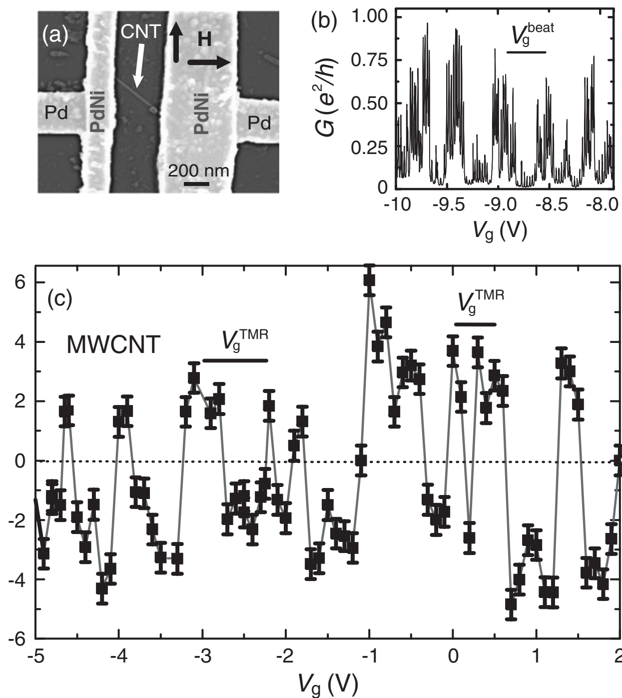

Figure 10. (*a*) SEM image of a CNT connected to FM PdNi contacts. The separation between the contacts is 400 nm. The magnetic field is applied parallel to the substrate, denoted by the arrows on the top right. (*b*) The linear conductance as a function of the gate voltage, measured at 300 mK. This figure shows a beating pattern with $\Delta V_g^{beat} \approx 0.4$ V. (*c*) MR values as a function of gate voltage for a MWCNT, measured at 1.85 K. The oscillations have a typical scale of 0.4 to 0.75 V, roughly corresponding to the beating pattern in (*b*). Courtesy of Sahoo *et al* [210].

believed to be half-metallic at low temperatures and to remain ferromagnetic at room temperature (see section 2.4). The 30 nm thick LSMO contacts are fabricated by pulsed laser deposition (PLD) and focused ion beam (FIB) milling. MWCNTs are then dispersed on the patterned substrate from solution and successfully contacted devices are selected. The room-temperature contact resistance of LSMO-CNT-LSMO devices is compared with Pd-CNT-Pd control devices and is found to be twice as high. The LSMO-CNT-LSMO devices show a conductance gap around zero bias voltage below 200 K, saturating to 250 mV at low temperature. Very recently, Hueso *et al* [213] reported a maximum MR ratio of 61% in a single MWCNT situated on top of two LSMO electrodes at 5 K. They find a spin relaxation time of 30 ns and a spin diffusion length of 50 μm. The MWCNT-LSMO interfaces behave like tunnel barriers, which is favourable for the spin signal, but should not matter if the polarization of LSMO is really 100% (see section 2.4). The tunnel barriers also limit the current, which allows for large-bias (∼25 mV) measurements. The relatively large-bias voltage circumvents the occurrence of Coulomb blockade and level quantization effects, and is a necessary condition for achieving large output signals. Their MR value corresponds to 65 mV, suitable for applications. The MR value drops to zero at 120 K, which is at a higher temperature than in earlier MWCNT devices.

Hoffer *et al* [214] have measured MWCNTs obtained by chemical vapour deposition (CVD) in porous alumina membranes. This fabrication method lacks the potential for gating the devices. Schneider *et al* report of a method for fabricating CNTs filled with FM materials (Co, Fe, Ni) [215]. It is a magnetic nanowire growth method as well as a new method for contacting electrodes to CNTs in spintronic devices of this kind. An alignment method for MWCNTs is proposed by Niyogi *et al* [216] in which CNTs end-capped with FM material can self-assemble on predefined FM contacts after introducing magnetic fields. This assembling technique could be relevant for actually realizing CNT-based spintronic devices.

4.2. *Single-wall carbon nanotubes*

SWCNTs possess some interesting characteristics as compared with MWCNTs for spin transport studies: less scattering (ballistic nature), well-defined band structure and enhanced Coulomb interaction [73]. SWCNTs form ideal 1D electronic systems for studying TLL behaviour (see section 1.4). On the other hand, SWCNTs are more difficult to reliably contact than MWCNTs, because of their smaller diameter and smaller mechanical stability [79,217]. SWCNTs are also more difficult to synthesise in large quantities, which makes them much more expensive as compared with MWCNTs [74].

Although *bundles* of SWCNTs (less than 10 nm in bundle diameter) contacted with Co electrodes have been very briefly discussed in [201], the interpretation of those data was difficult. The first report on single SWCNTs was published by Kim *et al*, who find a maximum MR of 3.4% at 0.2 K in Co/SWCNT/Co [217]. The SWCNTs are grown by CVD [218] on SiO_2. Co contacts are thermally evaporated on top of selected SWCNTs, after which a rapid thermal annealing is performed. The SWCNT is weakly coupled to the Co contacts and the authors expect there is a tunnelling barrier at the Co/SWCNT interfaces. The tunnel coupling results in quantum-dot behaviour, but the size of the Coulomb gap suggests that the dot size is not determined by the distance between the contacts but by disorder within the SWCNT. It is mentioned that SWCNTs with low-ohmic contacts do not show any MR. This could be due to the conductivity mismatch problem discussed in section 2.4, and thus indicates that the overall transport through the Co/SWCNT/Co system is diffusive. A spin relaxation length of 1.4 μm is estimated at 4.2 K, but also this estimate is based on only one contact separation (1.5 μm) and is therefore not very reliable. The MR does not decay with the contact separation, as the MR values for a 420 nm spacing are smaller than that of the 1.5 μm spacing.

Jensen *et al* fabricated SWCNTs by CVD on catalyst sites of Fe_2O_3/Mo supported by Al_2O_3 nanoparticles placed on a highly doped SiO_2/Si substrate [219]. The SWCNTs are contacted by Fe contacts capped with Au. The contact resistance in these devices is large as compared with devices with pure Au electrodes. They report 100% MR at 300 mK (60% at 4.2 K) in a Fe/SWCNT/Fe device [219].

Following their earlier experiments on SWCNTs, Jensen and coworkers reported on a new fabrication method in which SWCNTs are fully encapsulated in epitaxially grown heterostructures of GaAs/AlAs and (Ga,Mn)As, see figure 11 [220]. This is the first reported inorganic

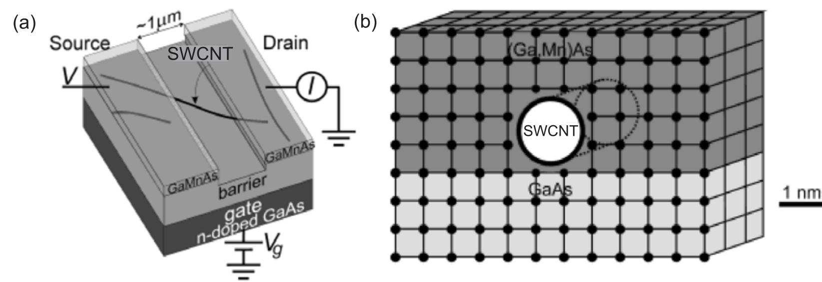

Figure 11. (*a*) Schematic picture of a SWCNT connected by two FM semiconductor contacts. The SWCNT is lying on a superlattice barrier and a heavily n-doped GaAs layer serves as a gate. The SWCNT is connected to two 30–50 nm thick islands of $Ga_{0.95}Mn_{0.05}As$ covered with a 3 nm GaAs layer to prevent oxidation. The separation between the two contacts is $\sim 1\ \mu$m. (*b*) Schematic image of the SWCNT encapsulated in the semiconductor crystal. Courtesy of Jensen *et al* [220].

hybrid semiconductor-CNT structure. The fabrication starts with an n-doped GaAs substrate (backgate) followed by a GaAs(2 nm)/AlAs (2 nm) superlattice (gate insulator), capped with 20 nm of epitaxial GaAs and a layer of amorphous As. Laser-ablated SWCNTs are then dispersed on top of the amorphous As layer, after which the amorphous As is evaporated in the MBE chamber, leaving the SWCNTs on a clean GaAs crystal surface. The SWCNTs are then overgrown by epitaxial $Ga_{0.95}Mn_{0.05}As$. A trench is etched in the GaMnAs layer, resulting in a SWCNT contacted by two GaMnAs contacts (see figure 11). The Curie temperature of the GaMnAs layer is ~ 70 K. In electron transport measurements Coulomb blockade is observed at low temperatures, as well as indications for TLL behaviour [220].

In a later publication [221], Jensen *et al* discuss MR measurements on these devices and compare them with devices with metallic FM contacts. At $T = 0.3$ K, a reproducible MR sign alteration is found in a small V_g-range. High MR ratios on the order of 100% have been reported. Somewhat troublesome, hysteretic MR was also found for devices with only one FM contact. Jensen *et al* cannot provide an explanation for the large MR, the sign change and the fact that MR also shows up with one FM contact.

The MWCNT measurements of Sahoo *et al*, discussed in section 4.1, were extended in the same study by measurements on SWCNTs. The results on SWCNTs were used to substantiate that interference of single-particle levels is the physical origin for the observed MR oscillation [210]. QD behaviour is already observed at 1.85 K in the SWCNTs (as compared with 0.3 K for the MWCNTs, see figure 10), as both the charging energy and the energy level spacing is larger for SWCNTs. The MR changes sign on each conductance resonance (see figure 12) and varies between -7% and 17%. The higher MR values as compared with the MWCNTs are ascribed to the larger charging energy in SWCNTs [222]. An order of magnitude lower MR is found for NM-SWCNT-NM control devices.

Sahoo *et al* explain the systematic change of MR sign with gate voltage by combining the spin-dependent Breit–Wigner formula for resonant tunnelling through a QD coupled to FM electrodes [223–225] with the Jullière TMR expression [142]. It is shown that on resonance the MR is negative, whereas off-resonance it is positive (see figure 12). For reproducing the observed asymmetry in the MR, it is assumed that the QD energy levels are spin-dependent, resulting in reasonable

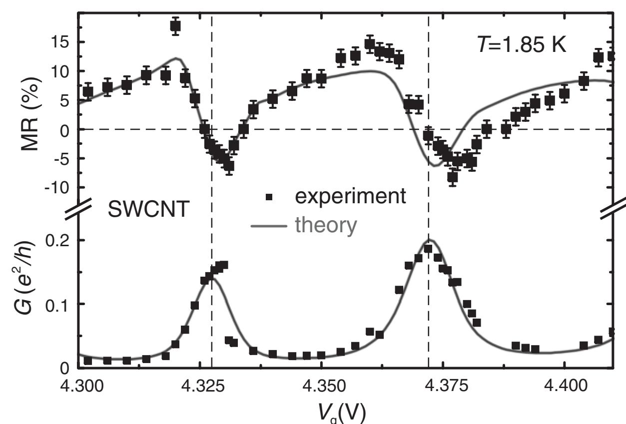

Figure 12. MR and linear conductance as a value of gate voltage for a SWCNT at 1.85 K. The separation between the contacts is 500 nm. The solid line gives a fit with the theory of the spin-dependent Breit–Wigner transmission probability. Courtesy of Sahoo *et al* [210].

agreement between experiment and theory. A quantitative theory based on the Landauer–Büttiker model describing the MR data, was presented in [226] and [227]. This model describes a quantum dot connected by two FM contacts. Depending on the magnetization of these contacts, carriers with different spins can pick up different phase shifts upon scattering, because they are affected by different scattering potentials. By taking into account the K–K' orbital degeneracy of a SWNT, the magnetoresistance as a function of the gate-voltage measured by Sahoo *et al* can be fitted. The only free parameter is the effective spin splitting of the dot energy levels due to the different phase shift of electrons scattering on an interface in the parallel P or AP configuration. MR measurements with a larger gate-voltage range could give more certainty about the validity of this model.

As opposed to the Coulomb blockade regime described above, Man and coworkers [228] have investigated a SWCNT connected to *highly transparent* PdNi contacts. In this regime, the SWCNT device acts like a Fabry–Pérot (quantum) interferometer, and not as a QD as in the case of [210]. The observed MR with a maximum of 4% at 4.2 K oscillates with gate voltage in phase with the resistance, which excludes magneto-Coulomb effects and can be fitted with a model based on the Landauer–Büttiker picture. Oscillations as a function of the bias voltage are also seen and can be understood in terms

Table 1. Reported MR values on CNT SV devices.

Nanotube	FM contacts	MR = $(R_{AP} - R_P)/R_P$ (%)	T (K)	References
MW	Co/Co	+9	4.2	[85]
MW	Co/Co	+2.5, +9	4.2	[202]
MW	Co/NiFe	−2.2, +0.6	14	[204]
MW	Co/Co	+30, −36	4.2	[205, 206]
MW	PdNi/PdNi	Oscillation from −5 to +6	1.85	[210]
MW	LSMO/LSMO	+40	4.2	[212]
MW	LSMO/LSMO	+61	5.0	[213]
MW	Co/Co	3.6	2.5	[214]
SW	PdNi/PdNi	Oscillation from −7 to +17	1.85	[210]
SW	LSMO/LSMO	+61	5.0	[213]
SW	Co/Co	+2.6	2.0	[217]
SW	Fe/Fe	+100	0.3	[219]
SW	(Ga,Mn)As/(Ga,Mn)As	75	0.3	[221]
SW	PdNi/PdNi	+4	4.2	[228]
SW	Co/Co	+6	4.2	[229]
SW	Ni/Ni	Oscillation from −6 to +10	4.2	[231]

of the model. Decrease of the MR with increasing bias is attributed to the decrease in polarization of the electrodes when the bias voltage approaches the exchange energy of PdNi.

As argued in section 2.5, there are a number of spurious effects that can obscure the MR due to the SV effect. In order to eliminate these spurious MR effects, Tombros *et al* for the first time used a 4-terminal, non-local geometry to measure spin accumulation in SWCNTs [229]. The non-local geometry (see figure 7) allows to separate the spin and charge currents and was successfully applied to inorganic (metallic) systems before [18, 165, 230]. Importantly, Tombros *et al* conclude that in their only working device the MR in conventional, two-terminal measurements (also applied in all experiments discussed so far) is dominated by spurious effects.

SWCNTs are deposited on a SiO_2 substrate, and Co contacts are fabricated using EB lithography and EB evaporation. In the non-local geometry, at least two out of the four contacts should be FM. For practical reasons, Tombros *et al* use four FM contacts with different coercive fields. It is essential that the contacts are low-ohmic (to avoid QD formation), and that charge and spin transport is possible beneath them. In their best device, a 4-terminal conductance of 2.5 e^2/h is measured, indicating that at least one metallic SWCNT is probed (bundles of a few SWCNT cannot be excluded however). Comparing the 2-terminal and 4-terminal resistances, contact resistances around a kΩ are deduced, much lower than in the case of, e.g. Tsukagoshi *et al* [85, 232]. Comparing the results of 2-terminal (local) and 4-terminal (non-local) measurements, it is concluded that 90% of the MR in the two-terminal measurement cannot be attributed to spin accumulation. Spin accumulation hence seems to be easily overshadowed by spurious effects.

Recently, Alphenaar's group has succeeded in contacting SWCNTs with Ni electrodes spaced 10 nm apart using shadow evaporation [231]. The comparison of these extremely short devices with earlier devices may shed more light on the role of spurious effects.

In addition to CNTs, also spin transport through C_{60} films is studied. Zare-Kolsaraki and Micklitz [233–237] studied MR in granular films of Co clusters mixed with C_{60} molecules. MR is observed in films with a Co fraction between 0.23 and 0.32. The highest MR they measure is around 30% at 4 K and drops to a few percent at 60 K. Miwa *et al* [238] studied the same system, but performed *ex situ* measurements (i.e. not under vacuum conditions as in the case of Zare-Kolsaraki and Micklitz), allowing for better characterization of their device. Good-quality devices give a MR of 8% at 4.2 K and around 0.1% at room temperature.

Recently also spin injection in graphene has been reported. Hill *et al* [239] measure a MR signal of 10% in a device consisting of a graphene sheet in between two large NiFe contacts. They rely on imperfections during fabrication to obtain contacts with different coercive fields.

4.3. Carbon nanotubes summary

An overview of spintronic experiments on CNTs is given in table 1. So far, MR is only observed at low temperatures with a maximum of 120 K in [213]. Metals (Co, NiFe, PdNi), half-metallic oxides (LSMO) and magnetic semiconductors (GaMnAs) have been used as FM contacts. Reasonably long spin relaxation times (up to 30 ns) and lengths (1.4–50 μm) have been derived. However, these numbers are not based on the MR signal for a reasonable amount of different contact separations (allowing for an exponential fit as explained in section 2.3.2). Instead, they are based on only one contact separation and (in most cases) the simple Jullière model, resulting most probably in underestimation of the spin relaxation time.

Although spin injection and detection in CNTs seems feasible, the large variation in obtained results is striking. Probably one of the major issues, if not *the* major issue, is the quality of the CNT-contact interface. Krompiewski [240] has shown that the GMR in a CNT depends on the detailed properties of the interface. Especially the introduction of an oxide layer in between the metal and the CNT, of which the coupling is assumed to be antiferromagnetic (as in the case of CoO, but also for NiO and FeO), can drastically influence the GMR ratio. The GMR signal also depends on the position of the chemical potential in the contacts.

For the case of MWCNTs, it is shown [241] that the GMR signal around E_F strongly depends on the interaction between the outer and the inner tubes (even when the current

flows solely through the outer shell). This may be one of the reasons for the observed negative GMR in some experiments. The degree of disorder in the CNT (impurities, dopants or incommensurate inner shells) has been identified as a cause of GMR reduction [242].

The gate-voltage dependence of the MR in CNTs has been studied for both weak coupling to the contacts (QD behaviour), as for transparent contacts (quantum interference behaviour). Some of these results can be explained in terms of the Landauer-Büttiker formalism, but more experimental work is needed to convincingly exclude spurious MR effects. The application of the non-local geometry of [229] may be crucial in this respect.

5. Experiments on organic thin-film, SAM and single-molecule devices

In this section, we discuss experiments on organic SV where the spacer between the FM electrodes is formed by an organic thin film. Thin films of polymers or small molecules are easy to fabricate and are already applied in different technological applications such as OLEDs (see section 1.1). The carrier mobility in organic thin films, however, is much lower than in CNTs. For measuring any sizeable MR effect in a SV structure, it is therefore necessary to have a small (∼100 nm) spacing between the FM contacts. Also experiments using single molecules and SAMs are discussed here.

5.1. Organic thin-film spin valves

An example of an organic semiconductor that is broadly applied in OLEDs is sexithienyl (T_6), a π-conjugated rigid-rod oligomer. Its HOMO level is 4.8 eV [243], and depending on its morphology, the mobility ranges from 10^{-2} to 10^{-4} cm^2 (V s)$^{-1}$ [244, 245]. Dediu *et al* [246] applied this p-type material in the first report on spin injection in an organic semiconducting film. Importantly, a MR effect was measured at *room temperature*. EB lithography is used to fabricate electrodes out of a thin (∼100 nm) film of $La_rSr_{1-r}MnO_3$ ($0.2 < r < 0.5$) deposited epitaxially on an insulating substrate, see figure 13. LSMO is a half-metal with ideally 100% spin-polarized carriers at the Fermi level below the Curie temperature ($T_C \sim 370$ K) (see section 2.4). Unlike FM contacts as Co, Ni or Fe, LSMO is stable against oxidation. The thin (100–150 nm) T_6 films are deposited on the substrate by molecular beam evaporation. The workfunction of LSMO is estimated to be around 5 eV, close to the HOMO level of T_6. The observed linear I–V characteristics seem to confirm the low-ohmic contact between LSMO and T_6. If the spin polarization in the LSMO contacts is indeed (close to) 100%, the conductivity mismatch problem (see section 2.4) should not play a role and the low-ohmic LSMO-T_6 contact should not prevent spin injection.

As the geometry (and hence the coercive field) of the LSMO electrodes is the same, Dediu *et al* do not succeed in switching the magnetization of each FM contact independently in a controlled fashion. However, they change the relative orientation from random, at low field, to parallel at higher field. A maximum resistance decrease of ∼30% from the random to the parallel configuration is observed for a 140 nm channel at room temperature. The MR is independent of field orientation (perpendicular or parallel), and no MR effect is observed for channels larger than 200 nm. The contact geometry complicates the evaluation of the spin relaxation length. A rough estimate of $l_s = 200$ nm is made. Using this value and a mobility of 10^{-4} cm^2 (V s)$^{-1}$, one finds a spin relaxation time $\tau_s \sim 1\ \mu$s.

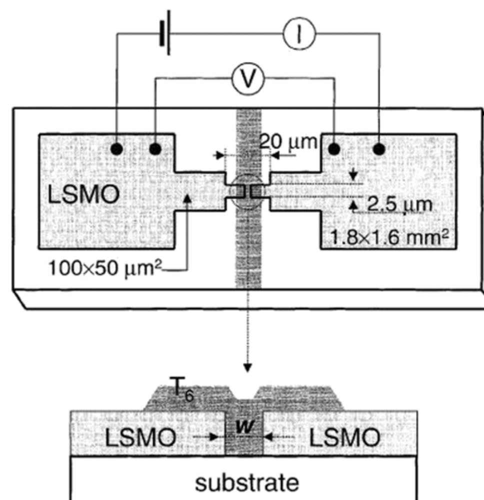

Figure 13. Schematic top view and cross section of a hybrid LSMO/T_6/LSMO junction. An epitaxial thin film of LSMO is deposited on matching substrates ($NdGaO_3$, $SrTiO_3$), and electrodes are fabricated by EB lithography. The separation w of the electrodes varies between 70 and 500 nm on one single substrate. T_6 films (100–150 nm thick) are deposited on top of the electrodes by molecular beam deposition. The resistance of the films is typically 10^2–10^3 for thicknesses of 100 nm. Reprinted from [246] courtesy of Dediu *et al* and with permission of Elsevier, copyright 2004.

Xiong *et al* [247, 248] used the small π-conjugated molecule 8-hydroxy-quinoline aluminium (Alq_3, see figure 2(*b*)) as a spacer in a (vertical) SV device, see figure 14(*a*). Alq_3 is a popular material for use in OLEDs, as it is easily deposited and can be combined with various metallic electrodes. LSMO is used as bottom contact ($H_c \sim 30$ Oe), and Co ($H_c \sim 150$ Oe) as the top electrode (see figure 14(*a*)). Xiong *et al* thereby succeeded in realizing both P and AP magnetization of the contacts. A schematic band diagram is given in figure 14(*b*), indicating the HOMO and LUMO levels of Alq_3 and the (nearly equal) workfunctions of LSMO and Co. At low bias voltages, holes are injected from the anode into the HOMO level. The evaporation of the top Co electrode causes pinholes and Co inclusions in the Alq_3 layer over a distance of ∼100 nm. The Co/Alq_3 interface is therefore poorly defined.

A *negative* MR of 40% is observed at 11 K for a 130 nm thick Alq_3 layer. Inverse MR has also been reported for LSMO/$SrTiO_3$/Co and LSMO/$Ce_{0.69}La_{0.31}O_{1.845}$/Co MTJs and is ascribed to negative spin polarization of the Co d-band. The MR strongly depends on bias voltage and temperature, and disappears for $|V| \gtrsim 1$ V, or $T \gtrsim 300$ K. The temperature dependence (figure 14(*c*)) is dominated by spin relaxation in Alq_3 (and not by the temperature dependence of the magnetization of the LSMO), as confirmed in SV devices where LSMO is replaced by Fe [249] and by photoluminescence measurements.

It is hard to make a good estimate for l_s in this geometry, but a value of ∼45 nm at 11 K is reported. The ill-defined

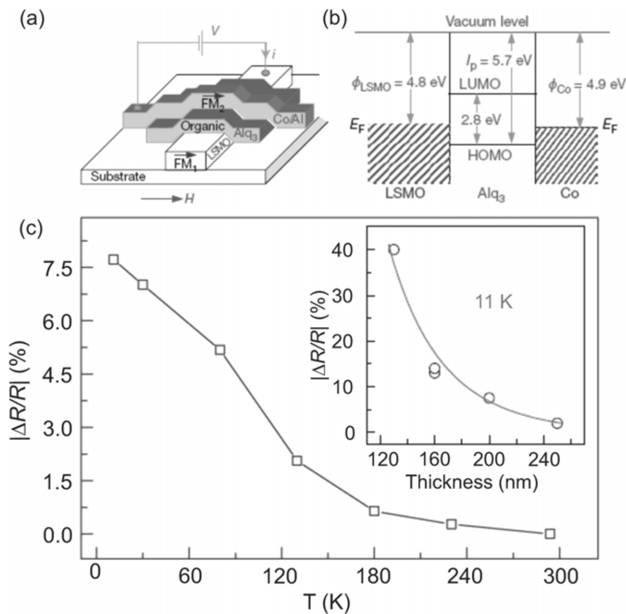

Figure 14. (*a*) Schematic picture of an organic SV device. For the bottom electrode (FM_1) a LSMO film is used, on which the organic semiconductor Alq_3 is thermally evaporated. A thin Co film (3–6 nm), serving as the second FM contacts (FM_2), and Al contact are then evaporated using a shadow mask without breaking the vacuum, resulting in an active device area of $2 \times 3\,mm^2$. A magnetic field is applied parallel to the substrate as denoted in the figure. (*b*) Schematic band diagram of this device in the rigid band approximation. The Fermi levels (E_F) and the workfunctions (ϕ) of LSMO and Co are shown, as well as the HOMO-LUMO levels of Alq_3. (*c*) MR as a function of temperature measured at a voltage of 2.5 mV for an Alq_3 thickness of 160 nm. The inset shows the MR as a function of thickness at a temperature of 11 K. The line through the data points is a three parameter fit to an adjusted Jullière model. Courtesy of Xiong *et al* [247].

Co/Alq_3 interface is somewhat troublesome in this experiment, and makes it difficult to interpret the results. As discussed in Part I, the role of the interfaces is extremely important in spintronic devices. Next to the low-T MR that is ascribed to the SV effect, a strong negative MR is observed for higher magnetic fields ($H = \sim$1–10 kOe) at higher temperature. The latter MR effect is referred to by the authors as *high-field magnetoresistance*, or HFMR. In a later work [250] it is argued that this HFMR can be related to the LSMO electrode (no HFMR is found in devices without LSMO contacts). Although single LSMO films already show HFMR, the effect is enhanced by orders of magnitude when the LSMO forms an interface with an organic semiconductor. For the proposed mechanism we refer to [250] and references therein.

Dediu *et al* find a considerable MR at room temperature (over a magnetic field scale of several kOe) in their LSMO/T_6/LSMO, whereas Xiong *et al* only find HFMR at higher temperatures (which is not related to the SV effect). The observed MR by Dediu and coworkers is therefore possibly also related to this HFMR. A distinction between GMR and HFMR could be made, by introducing asymmetry between the LSMO contacts in [246]. Room-temperature SV behaviour was also recently claimed in LSMO/P3HT/Co [251] and LSMO/P3OT/LSMO [252] devices, where P3HT is poly(3-hexyl thiophene) and P3OT is poly(3-octylthiophene), both semiconducting π-conjugated polymers.

Santos *et al* [253] demonstrate spin-polarized *tunnelling* through a thin Alq_3 barrier sandwiched between a Co (bottom) and $Ni_{80}Fe_{20}$ (permalloy, Py) contact (top) at *room temperature*. I–V- and polarization measurements indicate the good quality of the Alq_3 barrier without any Co inclusions. The TMR value is improved by adding an Al_2O_3 layer in between the Co and the Alq_3 tunnel barrier, which reduces the formation of interfacial charge states. The highest TMR they find at room temperature is 6% and a substantial TMR value is even present above 100 mV. They measure a positive polarization for Co and Py, which corresponds to the observed positive TMR, but is in contrast to the negative MR reported by Xiong *et al* [247]. Santos *et al* argue that this is not because of the negative polarization of the Co d-band, as proposed by Xiong *et al*, but might originate from the opposite spin asymmetry coefficients of Co and LSMO. They also state the role of the Co inclusions is unclear.

Riminucci *et al* [254] report on MR measurements on a vertical LSMO/Alq_3/tunnel barrier/Co device. The tunnel barrier is Al_2O_3 or LiF, and in both cases a negative MR of a few percent was detected up to 210 K. They especially focus on the interface between LSMO and Alq_3 in order to investigate the character of the charge carriers in Alq_3. Alq_3 is an n-type material, whereas the unperturbed energy levels suggest hole conduction. An explanation for the n-type behaviour is put forward by Lin *et al* [255]. They calculate the charge transfer integrals for electrons and holes and show that those for electrons can be more than ten times larger, due to the LUMO overlap of neighbouring atoms and the absence of HOMO overlap. Photo-electron spectroscopy reveals a strong interface dipole, which shifts the energy levels of the system. They construct a semi-quantitative energy level model which predicts electron transport due to a smaller energy barrier between the Fermi energy of LSMO and the LUMO of Alq_3 than between the Fermi energy and the HOMO level. The model also indicates a resonance between the LUMO level and the Co d-band, which provides an explanation for the negative SV effect.

A study of MR in Alq_3 *nanowires* has been performed by Pramanik *et al* [195]. They measured ensembles of Co/Alq_3/Ni nanowires (see figure 15(*a*)) and observed a MR effect of about 1% at low temperature (figure 15(*b*)). From their estimate of the spin relaxation length by the Jullière model they calculate the spin relaxation time, which turns out to be extremely long. Values between a few milliseconds and a second are obtained (see figure 15(*c*)), depending on what value is taken for mobility of the Alq_3, which is not exactly known.

The experiment by Pramanik *et al* [195] is the only experimental work so far that addresses the question which spin relaxation mechanism (see section 3) is dominant in organic semiconductors. It is argued that the DP mechanism is proportional to the carrier mobility, whereas the EY mechanism has an inverse dependence. Since it is more likely that the mobility has decreased in the nanowires as compared with bulk Alq_3, due to more Coulomb scattering at surface states, comparison between their results and that of Xiong and coworkers [247] gives an indication that the EY mechanism is dominant. However, the comparison is made between completely different experiments and the mobility is not explicitly measured. Therefore, more studies, also in

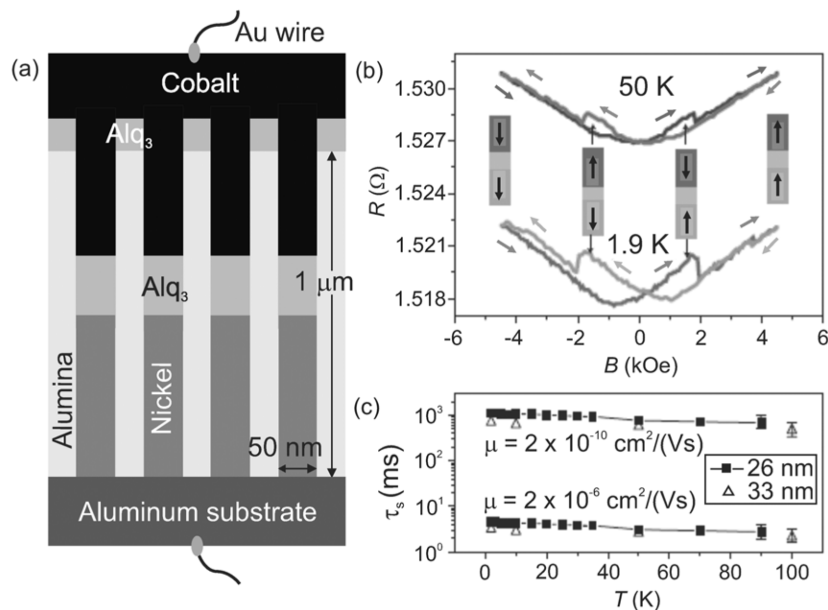

Figure 15. (*a*) Schematic picture of Alq_3 nanowires connected to Co and Ni electrodes. The nanowires with a diameter of 50 nm are synthesized in a porous Al membrane with a well-ordered hexagonal close-packed arrangement of 50 nm pores. (*b*) Forward and backward scan showing MR for two different temperatures. The magnetic field points parallel to the axis of the wires. (*c*) Calculated spin relaxation time as a function of temperature. The two curves give the maximum and minimum values. The large spread is caused by the spread in the reported mobility in the literature. Courtesy of Pramanik *et al* [195].

different organic systems, will be necessary to tell whether this conclusion is generally valid.

5.2. Organic magnetoresistance (OMAR)

Recently, there have been a number of studies—mainly by Mermer and Wohlgenannt and coworkers—reporting a considerable MR effect in organic semiconductor devices *without* FM contacts, referred to as 'organic magnetoresistance' or OMAR [177, 179, 252, 258–261]. In experiments on the polymer polyfluorene (PFO) [258], the small molecule Alq_3 [259] and several more π-conjugated polymers and small molecules [179], it was shown that this OMAR (defined as $\Delta R/R = R(B) - R(0)/R(0)$) is quite universal in nature, can be either positive or negative and reaches values up to 10% for $B \sim 10$ mT at room temperature. OMAR is shown to be related to the bulk resistance of the organic film [258, 259]. Depending on the organic material, OMAR obeys the empirical law $\Delta R(B)/R \propto B^2/(B^2 + B_0^2)$ or $\Delta R(B)/R \propto B^2/(|B| + B_0)^2$, where $B_0 \approx 5$ mT in most materials [179], increasing with spin–orbit coupling. The effect is only weakly dependent on temperature, is independent of magnetic field direction and impurities and typically decreases with increasing voltage and carrier density [258, 259]. It was argued that OMAR is a bulk effect related to the majority carrier current only (holes in PFO and electrons in Alq_3). In [260] hyperfine interaction (see section 3.2) was explored as a possible cause of OMAR. Although the model presented could explain some characteristics of OMAR, open questions remained.

Prigodin *et al* [177] recently proposed a model to explain OMAR based on the assumption that charge transport in organic semiconductors is electron–hole recombination limited. It is argued that in the space-charge-limited transport regime (i.e. there are no free carriers induced by a gate as in an OTFT, see section 2), both electrons and holes are injected (possibly with very different mobilities). The electron and holes can form electron–hole (e–h) pairs, that are either in the singlet (S) or triplet (T) state. It is shown that the space-charge-limited current density increases with decreasing e–h recombination rate. As the recombination rate depends on the degree of mixing between S and T states, the recombination rate—and hence the current density—becomes B-dependent. However, the experimental fact that OMAR is weakly dependent on the minority carrier density (and also occurs in heavily p-doped devices) is not in agreement with the Prigodin model.

Another model has been put forward by Wohlgennant [261]. In this paper, OMAR is explained by hopping, which is restricted by Pauli blockade. Hopping from a single occupied (SO) state to another SO state, forming a double occupied (DO) state, is not allowed when the spins are parallel, due to the Pauli principle. The chance of a hopping event is therefore proportional to the singlet probability of two SO states. Applying an external magnetic field sets a global quantization axis for the spins of the carriers, which are quantized along a local axis, set by the local hyperfine field, without this magnetic field. In the absence of the field, hops are allowed between all SO sites with a certain probability, but due to the global quantization axis Pauli blockade decreases the number of hopping events. Monte Carlo simulations based on this theory show good agreement with measured data. An increase in the current might be explained by the fact that immobile bipolaron formation restricts the mobile polarons to a smaller volume, thereby increasing the carrier density.

5.3. Single-molecule devices and self-assembled monolayers

Although the organic semiconductor devices described above have very thin layers of polymers or small molecules, these

Table 2. Reported MR values on organic thin-film, SAM and single-molecule devices.

Material	FM contacts	MR $= (R_{AP} - R_P)/R_P$ (%)	T (K)	References
T_6	LSMO/LSMO	+30	300	[246]
Alq_3	LSMO/Co	40	11	[247]
P3HT	LSMO/Co	80/1.5	5/300	[251]
Alq_3 (tunnel barrier)	Co-Al_2O_3/Py	+6	300	[253]
Alq_3 (tunnel barrier)	LSMO/Al_2O_3,LiF-Co	−2.5	100	[254]
Alq_3 (nanowires)	Co/Ni	1	1.9–100	[195]
Octanedithiol	Ni/Ni	−6 to +16	4.2	[266]

layers are still typically thicker than ∼100 nm. In the search for miniaturization of electronic functional devices, molecular monolayers, and eventually single molecules are the ultimate limit (see section 1.3). The spintronic properties of such systems have not been explored extensively yet, but a few interesting studies are discussed below.

Using time-resolved Faraday rotation spectroscopy, Ouyang and Awschalom demonstrated coherent spin transfer of photo-excited carriers between semiconductor QDs through conjugated molecules at room temperature [262]. Their devices consist of multilayer CdSe QDs solids that are bridged by 1,4-benzenedimethanethiol, and they show that the spin transfer efficiency is ∼20%.

Pasupathy *et al* [263] have observed the Kondo [264, 265] effect in single C_{60} molecules connected to two Ni electrodes. The electrodes are made by electromigration after which a solution of C_{60} is dispersed onto them. Different shapes of the contacts allow for independent switching of their magnetization. The Kondo behaviour is confirmed by the dependence of the conductance on the temperature and the magnetic field. TMR values of −38% and −80% are found, much larger than the predicted value of 21% by the Jullière model, which is explained by the fact that for AP magnetization, the Kondo resonance occurs closer to the Fermi energy, thereby enhancing its conductance.

The first transport measurements on a SV involving a single molecular layer were reported by Petta *et al* [266]. The device is a nanometre-scale magnetic tunnel junction in the nanopore geometry [267, 268], consisting of a SAM of octanedithiol (100–400 molecules) sandwiched in between Ni contacts. The transport properties of octanethiol with NM contacts have been extensively studied [269–272].

The majority of the octanedithiol devices have resistances larger than h/e^2, implying tunnelling transport. A tunnelling barrier height of 1.5 eV is found in reasonable agreement with earlier work on octanethiols on Au [272]. Both positive and negative MR up to 16% is reported for low bias voltage at 4.2 K, rapidly decreasing with bias voltage and temperature. The largest MR is measured for the most resistive devices. The Jullière formula (using the definition TMR $= R_{max} - R_{min}/R_{min}$) is TMR $= 2P_1P_2/(1 - P_1P_2)$. Using $P_1 = P_2 = 0.31$ for Ni, one finds TMR = 21%, somewhat larger than the experimentally observed MR values. Several test devices are made in order to rule out artefacts of the fabrication process. As mentioned in section 2.2, localized states in the SAM tunnel barrier could possibly explain the anomalous behaviour. Also the observed telegraph noise may be due to imperfections in the molecular barrier.

In [138] Rocha calculates the transport properties through two different molecules sandwiched between two FM leads. They predict both TMR and GMR behaviour for octane and 1,4-[n]-phenyl-dithiolate, respectively.

One step further than the above work of Petta *et al* would be to integrate the spintronic functionality *within* the molecule. Liu *et al* [273] have proposed a single-molecule spin switch and SV based on the organometallic molecule dicobaltocene between NM contacts. The singlet (AP) spin state blocks electron transport near the Fermi energy, while the triplet (P) state enables much higher current. The S–T energy splitting depends on the insulating spacer between the cobaltocenes.

5.4. Organic thin-film, SAM and single-molecule devices summary

MR has been reported in a few organic semiconductors at different temperatures (table 2). Although the mobilities in these materials are rather low, reasonably large spin relaxation lengths (100–200 nm) and accompanying large spin relaxation times (1 μs) have been reported. These values are however still rough estimates. The experiments seem promising for spin injection into organic semiconductors, but some remarks have to be made. In the case of the early T_6 experiment [246], the symmetry of the two contacts makes the interpretation of the data difficult. HFMR has also been suggested to be the origin of the observed effect. For the Alq_3 experiments, EB evaporation of the top contacts most probably introduces impurities in the material. Non-destructive contacting is need for extracting reliable values for the spin relaxation length and time.

A few experimental studies exist on spin transport through a SAM or single molecule. These experiments are very interesting from a fundamental point of view and could provide more information about tunnelling and transport mechanisms in organic spintronic devices.

OMAR has been observed in organic semiconducting devices without FM contacts. A theoretical model for this effect is provided, but more research is needed to find the exact mechanism for this effect.

6. Conclusions

Since the first reported organic spintronic device in 1998, devices with a variety of organic spacer materials have been experimentally investigated. Most research so far has been devoted to CNTs. They offer low spin–orbit coupling and hyperfine interaction (and hence expectedly long spin relaxation times) in combination with high carrier mobilities. In addition, CNTs allow for studying the interplay of spin transport with Coulomb charging and quantum interference effects. Organic thin films have been investigated and there are a few studies on spin-dependent tunnelling through SAMs and

single-molecule structures. Thin-film devices are receiving an increasing amount of attention, not in the last place because of the recent discovery of OMAR in organic semiconductors. The recently discovered 2D form of carbon, graphene, is very promising for spintronic research as well as for the realization of spin-based quantum bits.

Although a lot of promising results have been obtained in the last decade, there are still a number of serious problems to be tackled. Control and understanding of the ferromagnet-organic interface is one of the major issues. Because of the fragile nature of organic materials, conventional microfabrication techniques cannot be used without caution. Non-destructive contacting of organic materials is important in organic electronics in general, but of crucial importance in organic spintronics in particular. A lot of effort is needed in this direction. Besides reliable contacts, also well-defined and clean organic spacer materials are needed. Defects and impurities in the organic materials themselves are certainly also a cause of the large scatter in the observed MR values. Even in the absence of defects or impurities, the combination of different materials can lead to new behaviour, for example due to the formation of an interface dipole layer.

Most spin relaxation lengths reported so far for organic devices are comparable to metals and inorganic semiconductors. The largest relaxation length [213] is however an order of magnitude larger than electrically detected in GaAs (6 μm) [12] and almost two others of magnitude larger than that electrically measured for metals (around 1 μm at 4.2 K and several hundreds of nm at room temperature [18]). However, these values have to be considered with a little care. Most of the time, the relaxation length is obtained with a modified Jullière model for only one contact spacing and therefore does not account for spin relaxation at the interface. A more elaborate model, like the one provided by Jaffrès and Fert [166], could lead to more accurate calculations. Length-dependent studies, in which the injector–detector distance is varied within the same device, are necessary. Another problem is separating true SV signals from spurious effects. A way to undoubtedly rule out other effects is a non-local measurement, where pure spin accumulation is measured. The study of spin injection, transport and relaxation in organic materials is still in its infancy. There is still a lot to find out about the role of the transport mechanism (band or hopping conduction, polaronic transport) on spin transport. Especially for finding the relevant spin relaxation mechanisms in organic materials, more theoretical and experimental work is needed.

The discovery of TMR and GMR in metallic spin valves has led to a revolution in magnetic memory. Parallel to this, the application of organic materials for electronic devices meant another revolution. The merging of spintronics and organic electronics is likely to ultimately lead to new spin-based, versatile devices and possibly even to robust quantum bits for quantum information and computation. Along the way, certainly many fundamental issues need to be addressed, being a challenge for scientists from different disciplines. Organic spintronics is an area of research where physics, chemistry and electrical engineering inevitably meet, and is hence an intriguing interdisciplinary field of research.

Acknowledgments

We thank R Coehoorn, V Dediu, R Jansen, M P de Jong, L P Kouwenhoven, C Schönenberger, K Tsukagoshi, L M K Vandersypen, and B J van Wees for fruitful discussions. This work is part of the VIDI research programme 'Organic materials for spintronic devices', financially supported by the Netherlands Organisation for Scientific Research (NWO) and the Technology Foundation STW.

References

[1] Farchioni R and Grosso G 2001 *Organic Electronic Materials* (Berlin: Springer)
[2] Cuniberti G, Fagas G and Richter K (ed) 2005 *Introducing Molecular Electronics* (Berlin: Springer)
[3] Klauk H (ed) 2006 *Organic Electronics: Materials, Manufacturing and Applications* (Weinheim: Wiley-VCH)
[4] Prinz G A 1995 *Phys. Today* **48** 58
[5] Prinz G A 1998 *Science* **282** 1660
[6] Wolf S A, Awschalom D D, Buhrman R A, Daughton J M, von Molnár S, Roukes M L, Chtchelkanova A Y and Treger D M 2001 *Science* **294** 1488
[7] Das Sarma S 2001 *Am. Sci.* **89** 516
[8] Gregg J F, Petej J, Jouguelet E and Dennis C 2002 *J. Phys. D: Appl. Phys.* **35** R121
[9] Zutič I, Fabian J and Das Sarma S 2004 *Rev. Mod. Phys.* **76** 323
[10] Awschalom D D and Flatté M E 2007 *Nature Phys.* **3** 153
[11] Thomson W 1857 *Proc. R. Soc. Lond.* **8** 546
[12] Lou X, Adelmann C, Crooker S A, Garlid E S, Zhang J, Reddy S M, Flexner S D, Palmstrøm C J and Crowell P A 2007 *Nature Phys.* **3** 197
[13] Miller J S and Epstein A J 1994 *Angew. Chem. Int.* **33** 385
[14] Miller J S 2000 *Inorg. Chem.* **39** 4392
[15] Blundell S J and Pratt F L 2004 *J. Phys.: Condens. Matter* **16** R771–828
[16] Sanvito S and Rocha A R 2006 *J. Comput. Theor. Nanosci.* **3** 624
[17] Krinichnyi V I 2000 *Synth. Met.* **108** 173
[18] Jedema F J, Filip A T and van Wees B J 2001 *Nature* **410** 345
[19] Fert A and Jaffrès H 2002 *Phys. Rev.* B **64** 184420
[20] Fert A, George J-M, Jaffrès H and Mattana R 2006 *Preprint* cond-mat/0612495
[21] Kikkawa J M, Smorchkova I P, Samarth N and Awschalom D D 1997 *Science* **277** 1284
[22] Kikkawa J M and Awschalom D D 1998 *Phys. Rev. Lett.* **80** 4313
[23] Kikkawa J M and Awschalom D D 1999 *Nature* **397** 139
[24] Malajovich I, Kikkawa J M, Awschalom D D, Berry J J and Samarth N 2000 *Phys. Rev. Lett.* **84** 1015
[25] Arisi E, Bergenti I, Dediu V, Loi M A, Muccini M, Murgia M, Ruani G, Taliani C and Zamboni R 2003 *J. Appl. Phys.* **93** 7682
[26] Bergenti I, Dediu V, Murgia M, Riminucci A, Ruani G and Taliani C 2004 *J. Lumin.* **110** 384
[27] Hayer A, Köhler A, Arisi E, Bergenti I, Dediu A, Taliani C, Al-Suti M and Khan M S 2004 *Synth. Met.* **147** 155
[28] Davis A H and Bussmann K 2003 *J. Appl. Phys.* **93** 7358
[29] Petty M C, Bryce M R and Bloor D (eds) 1995 *An Introduction to Molecular Electronics* (Oxford: Oxford University Press)
[30] Voss D 2000 *Nature* **407** 442
[31] Reese C, Roberts M, Ling M M and Bao Z 2004 *Mater. Today* **7** 20
[32] Forrest S R 2004 *Nature* **428** 911
[33] de Boer R W I, Gershenson M E, Morpurgo A F and Podzorov V 2004 *Phys. Status. Solidi.* a **201** 1302
[34] see e.g. http://www.polymervision.nl/

[35] Sze S M 1981 *Physics of Semiconductor Devices* (New York: Wiley-Interscience)
[36] Facchetti A 2007 *Mater. Today* **10** 28
[37] Ruden P P and Smith D L 2004 *J. Appl. Phys.* **95** 4898–904
[38] Tang C W and van Slyke S A 1987 *Appl. Phys. Lett.* **51** 913
[39] Friend R H *et al* 1999 *Nature* **397** 121–8
[40] Brabec C J, Sariciftci N S and Hummelen J C 2001 *Adv. Funct. Mater.* **11** 15–26
[41] Peumans P, Uchida S and Forrest S R 2003 *Nature* **425** 158–62
[42] Sirringhaus H *et al* 1999 *Nature* **401** 685–8
[43] Dimitrakopoulos C D and Malenfant P R L 2002 *Adv. Mater.* **14** 99-117
[44] Bolto B A, McNeill R and Weiss D E 1963 *Aust. J. Chem.* **16** 1090
[45] Chiang C K, Fincher Jr C R, Park Y W and Heeger A J 1977 *Phys. Rev. Lett.* **39** 1098
[46] Shirakawa H, Louis E J, MacDiarmid A G, Chiang C K and Heeger A J 1977 *J. Chem. Soc. Chem. Commun.* **16** 578
[47] McCulloch I *et al* 2006 *Nature* **5** 328
[48] Dhoot A S, Yuen J D, Heeney M, McCulloch I, Moses D, Heeger A J 2006 *Proc. Natl. Acad. Sci. USA* **103** 11834
[49] Sirringhaus H, Tessler N and Friend R H 1998 *Science* **280** 1741
[50] de Boer R W I 2005 *PhD Thesis* (Delft: Ponsen & Looijen)
[51] Salleo A 2007 *Mater. Today* **10** 38
[52] Peierls R E 1955 *Quantum Theory of Solids* (Oxford: Oxford University Press)
[53] Wang G M, Swensen J, Moses D and Heeger A J 2003 *J. Appl. Phys.* **93** 6137
[54] Campbell I H, Kress J D, Martin R L, Smith D L, Barashkov N N and Ferraris J P 1997 *Appl. Phys. Lett.* **71** 3528
[55] Silinsh E A and Čapek V 1994 *Organic Molecular Crystals: Interaction, Localization, and Transport Phenomena* (New York: AIP)
[56] Sundar V C, Zaumseil J, Podzorov V, Menard E, Willett R L, Someya T, Gershenson M E and Rogers J A 2004 *Science* **303** 1644
[57] Reese C and Bao Z 2007 *Mater. Today* **10** 20
[58] Brocks G, van den Brink J and Morpurgo A F 2004 *Phys. Rev. Lett.* **93** 146405
[59] Jurchescu O D, Baas J and Palstra T T M 2004 *Appl. Phys. Lett.* **84** 3061
[60] Podzorov V, Menard E, Borissov A, Kiryukhin V, Rogers J A and Gershenson M E 2004 *Phys. Rev. Lett.* **93** 086602
[61] Mas-Torrent M and Rovira C 2006 *J. Mater. Chem.* **16** 433
[62] Laudise R A, Kloc C, Simpkins P G and Siegrist T 1998 *J. Cryst. Growth* **187** 449
[63] Briseno A L, Mannsfeld S C B, Ling M M, Liu S, Tseng R J, Reese C, Roberts M E, Yang Y, Wudl F and Bao Z 2006 *Nature* **444** 913
[64] Aviram A and Ratner M A 1974 *Chem. Phys. Lett.* **29** 277
[65] Szent-Györgyi A 1941 *Nature* **148** 157
[66] Reed M A, Zhou C, Muller C J, Burgin T P and Tour J M 1997 *Science* **278** 252
[67] Dadosh T, Gordin Y, Krahne R, Khivrich I, Mahalu D, Frydman V, Sperling J, Yacoby A and Bar-Joseph I 2005 *Nature* **436** 677
[68] Hipps K W 2001 *Science* **294** 536
[69] Chen J, Reed M A, Rawlett A M and Tour J M 1999 *Science* **286** 1550
[70] Park J-H, Vescovo E, Kim H-J, Kwon C, Ramesh R, Venkatesan T 1998 *Nature* **392** 794
[71] Cui X D, Primak A, Zarate X, Tomfohr J, Sankey O F, Moore A L, Moore T A, Gust D, Harris G and Lindsay S M 2001 *Science* **294** 571
[72] Dekker C 1998 *Phys. Today* **52** 22
[73] Dresselhaus M, Dresselhaus G and Avouris P (ed) 2001 *Carbon Nanotubes: Synthesis, Structure, Properties, and Applications* (Springer: Berlin)
[74] Baughman R H, Zakhidov A A and de Heer W A 2002 *Science* **297** 787
[75] Iijima S 1991 *Nature* **354** 56
[76] Geim A K and Novoselov K S 2007 *Nature Mater.* **6** 183
[77] Saito R, Dresselhaus M S and Dresselhaus G 1998 *Physical Properties of Carbon Nanotubes* (Singapore: World Scientific)
[78] Frank S, Poncharal P, Wang Z L and de Heer W A 1998 *Science* **280** 1774
[79] Schönenberger C, Bachtold A, Strunk C, Salvetat J-P and Forro L 1999 *Appl. Phys. A: Mater. Sci. Process.* **A69** 283
[80] Postma H W Ch, Teepen T, Yao Z, Grifoni M and Dekker C 2001 *Science* **293** 76
[81] Rueckes T, Kim K, Joselevich E, Tseng G Y, Cheung C and Leiber C M 2000 *Science* **289** 94
[82] Avouris P 2002 *Acc. Chem. Res.* **35** 1026
[83] Joachim C, Gimzewski J K and Aviram A 2000 *Nature* **408** 541
[84] Menon M and Srivastava D 1998 *J. Mater. Res.* **13** 2357
[85] Tsukagoshi K, Alphenaar B W and Ago H 1999 *Nature* **401** 572
[86] Tomonaga S 1950 *Prog. Theor. Phys.* **5** 544
[87] Luttinger J M 1963 *J. Math. Phys.* **4** 1154
[88] Balents L and Egger R 2001 *Phys. Rev.* B **64** 035310
[89] Tokura Y, van der Wiel W G, Obata T and Tarucha S 2006 *Phys. Rev. Lett.* **96** 047202
[90] Loss D and DiVincenzo D P 1998 *Phys. Rev.* A **57** 120
[91] Zuppiroli L, Bussac M N, Paschen S, Chauvet O and Forro L 1994 *Phys. Rev.* B **50** 5196
[92] Vissenberg M C J M and Matters M 1998 *Phys. Rev.* B **57** 12964
[93] Nelson S F, Lin Y-Y, Gundlach D J and Jackson N 1998 *Appl. Phys. Lett.* **72** 1854
[94] Coehoorn R 2005 *Phys. Rev.* B **72** 155206
[95] Pasveer W F, Cottaar J, Tanase C, Coehoorn R, Bobbert P A, Blom P W M, de Leeuw D M and Michels M A J 2005 *Phys. Rev. Lett.* **94** 206601
[96] Hannewald K, Stojanović V M, Schellekens J M T and Bobbert P A 2004 *Phys. Rev.* B **69** 075211
[97] Horowitz G 2003 *Adv. Funct. Mater.* **13** 3
[98] Chua L-L, Zaumseil J, Chang J-F, Ou E C-W, Ho P K-H, Sirringhaus H and Friend R H 2005 *Nature* **434** 194
[99] Jarrett C P, Pichler K, Newbould R and Friend R H 1996 *Synth. Met.* **77** 35
[100] Kobayashi S, Takenobu T, Mori S, Fujiwara A and Iwasa Y 2003 *Appl. Phys. Lett.* **82** 4581
[101] Katz H E, Lovinger A J, Johnson J, Kloc C, Siegrist T, Li W, Lin Y Y and Dodabalapur A 2000 *Nature* **404** 478
[102] Malenfant P R L, Dimitrakopoulos C D, Gelorme J D, Kosbar L L, Graham T O, Curioni A and Andreoni W 2002 *Appl. Phys. Lett.* **80** 2517
[103] de Boer R W I, Iosad N N, Stassen A F, Klapwijk T M and Morpurgo A F 2005 *Appl. Phys. Lett.* **86** 032103
[104] Pope M and Swenberg C E 1999 *Electronic Processes in Organic Crystals and Polymers* (New York: Oxford University Press)
[105] Brazovskii S A and Kirova N N 1981 *Sov. Phys.—JETP* **33** 4
[106] Chance R R, Brédas J L and Silbey R 1984 *Phys. Rev.* B **29** 4491
[107] Johansson Å and Stafström S 2001 *Phys. Rev. Lett.* **86** 3602
[108] Fu J-Y, Ren J-F, Liu X-J, Liu D-S and Xie S-J 2006 *Phys. Rev.* B **73** 195401
[109] Wei J H, Xie S J, Mei L M, Berakdar J and Yan Y-J 2006 *New Journal of Physics* **8** 82
[110] Wei J H, Xie S J, Mei L M and Yan Y-J 2005 *Preprint* cond-mat/0508417
[111] Stoneham A M, Ramos M M D, Almeida A M, Correira H M G, Ribeiro R M, Ness H and Fischer A J 2002 *J. Phys.: Condens. Matter* **14** 9877
[112] Bussac M N, Picon J D and Zuppiroli L 2004 *Europhys. Lett.* **66** 392

[189] Bennati M, Nemeth K, Surján P R and Mehring M 1996 *J. Chem. Phys.* **105** 4441
[190] Coehoorn R 2006 private communication
[191] Dresselhaus G 1955 *Phys. Rev.* **100** 580
[192] D'yakonov M I and Perel V I 1971 *Sov. Phys.—JETP* **33** 1053
[193] Bychkov Yu A and Rashba E I 1984 *JETP Lett.* **39** 78
[194] Elliot R J 1954 *Phys. Rev.* **96** 266
[195] Pramanik S, Stefanita C-G, Patibandla S, Bandyopadhyay S, Garre K, Harth N and Cahay M 2007 *Nature Nanotech.* **2** 216
[196] Pramanik S, Bandyopadhyay S, Garre K and Cahay M 2006 *Phys. Rev.* B **74** 235329
[197] Bir G L, Aronov A G and Pikus G E 1976 *Sov. Phys.—JETP* **42** 705
[198] Merkulov I A, Efros A L, Rosen J 2002 *Phys. Rev.* B **65** 205309
[199] Khaetskii A V, Loss D and Glazman L 2002 *Phys. Rev. Lett.* **88** 186802
[200] Cottet A, Kontos T, Sahoo S, Man H T, Choi M-S, Belzig W, Bruder C, Morpurgo A F and Schönenberger C 2006 *Semicond. Sci. Technol.* **21** S78
[201] Tsukagoshi K and Alphenaar B W 2000 *Superlatt. and Microstruct.* **27** 565
[202] Chakraborty S, Walsh K M, Alphenaar B W, Lei L and Tsukagoshi K 2003 *Appl. Phys. Lett.* **83** 1008
[203] Alphenaar B W, Tsukagoshi K and Wagner M 2001 *J. Appl. Phys.* **89** 6863
[204] Orgassa D, Mankey G J and Fujiwara H 2001 *Nanotechnology* **12** 281
[205] Zhao B, Monch I, Vinselberg H, Muhl T and Schneider C M 2002 *Appl. Phys. Lett.* **80** 3144
[206] Zhao B, Monch I, Muhl T, Vinselberg H and Schneider C M 2002 *J. Appl. Phys.* **91** 7026
[207] Ishiwata Y, Maki H, Tsuya D, Suzuki M and Ishibashi K 2005 *Phys. Status. Solidi.* c **2** 3137
[208] Sahoo S, Kontos T, Schonenberger C and Surger C 2005 *Appl. Phys. Lett.* **86** 112109
[209] Javey A, Guo J, Wang Q, Lundstrom M and Dai H 2003 *Nature* **424** 654
[210] Sahoo S, Kontos T, Furer J, Hoffmann C, Graber M, Cotter A and Schönenberger C 2005 *Nature Phys.* **1** 99-102
[211] Schäpers Th, Nitta J, Heersche H B and Takayanagi H 2001 *Phys. Rev.* B **64** 125314
[212] Hueso L E *et al* 2006 *Appl. Phys. Lett.* **88** 083120
[213] Hueso L E, Pruneda J M, Ferrari V, Burnell G, Valdés-Herrera J P, Simons B D, Littlewood P B, Artacho E, Fert A and Mathur N D 2007 *Nature* **445** 410
[214] Hoffer X, Klinke C, Bonard J M, Gravier L and Wegrowe J E 2004 *Europhys. Lett.* **67** 103
[215] Schneider C M *et al* 2004 *Diamond Relat. Mater.* **13** 215
[216] Niyogi S, Hangarter C, Thamankar R M, Chiang Y F, Kawakami R, Myung N V and Haddon R C 2004 *J. Phys. Chem.* B **108** 19818
[217] Kim J R, So H M, Kim J J and Kim J 2002 *Phys. Rev.* B **66** 233401
[218] Kong J, Soh H T, Cassell A M, Quate C F and Dai H 1998 *Nature* **395** 878
[219] Jensen A, Nygård J and Borggreen J 2003 *Proc. Int. Symp. on Mesoscopic Superconductivity and Spintronics* ed H Takayanagi and J Nitta (Singapore: World Scientific) p 33
[220] Jensen A, Hauptmann J R, Nygård J, Sadowski J and Lindelof P E 2004 *Nano Lett.* **4** 349
[221] Jensen A, Hauptmann J R, Nygård J and Lindelof P E 2005 *Phys. Rev.* B **72** 035419
[222] Barnas J, Martinek J, Michalek G, Bulka B R and Fert A 2000 *Phys. Rev.* B **62** 12363
[223] Brataas A, Nazarov Yu V and Bauer G E W 2000 *Phys. Rev. Lett.* **84** 2481
[224] Waintal X, Myers E B, Brouwer P W and Ralph D C 2000 *Phys. Rev.* B **62** 12317
[225] Braun M, König J and Martinek J 2004 *Phys. Rev.* **70** 195345
[226] Cottet A, Kontos T, Belzig W, Schönenberger C and Bruder C 2006 *Europhys. Lett.* **74** 320
[227] Cottet A and Choi M-S 2006 *Phys. Rev.* B **74** 235316-1
[228] Man H T, Wever I J W and Morpurgo A F 2006 *Phys. Rev.* B **73** 241401(R)
[229] Tombros N, Molen S J van der and van Wees B J 2006 *Phys. Rev.* B **73** 233403
[230] Jedema F J, Heersche H B, Filip A T, Baselmans J J A and van Wees B J 2002 *Nature* **416** 713
[231] Nagabhirava B, Bansal T, Sumanasekera G, Lei Liu and Alphenaar B W 2006 *Appl. Phys. Lett.* **88** 023503
[232] Tsukagoshi K, Alphenaar B W and Ago H 2000 *Physica* E **6** 848
[233] Zare-Kolsaraki H and Micklitz H 2003 *Phys. Rev.* B **67** 224427
[234] Zare-Kolsaraki H and Micklitz H 2004 *Eur. Phys. J.* B **40** 103-109
[235] Zare-Kolsaraki H and Micklitz H 2004 *J. Magn. Magn. Mater.* **280** 311
[236] Zare-Kolsaraki H and Micklitz H 2003 *Phys. Rev.* B **67** 094433
[237] Zare-Kolsaraki H and Micklitz H 2006 *J. Magn. Magn. Mater.* **296** 9-12
[238] Miwa S, Shiraishi M, Mizuguchi M, Shinjo T and Suzuki Y 2006 *Japan. J. Appl. Phys.* **45** L717
[239] Hill E W, Novoselov K, Schedin F and Blake P 2006 *IEEE Trans. Magn.* **42** 2694
[240] Krompiewski S 2004 *J. Phys.: Condens. Matter* **16** 2981
[241] Krompiewski S 2005 *Phys. Status. Solidi.* B **242** 226
[242] Krompiewski S, Nemec N and Cuniberti G 2006 *Phys. Status. Solidi.* B **243** 179
[243] Hill I G, Kahn A, Soos Z G and Pascal Jr R A 2000 *Chem. Phys. Lett.* **327** 181
[244] Torsi L, Dodapalapur A, Rothberg L J, Fung A W P, and Katz H E 1998 *Phys. Rev.* B **57** 2271
[245] Ostoja P, Guerri S, Impronta M, Zabberoni P, Danieli R, Rossini S, Taliani C and Zamboni R 1992 *Adv. Mater. Opt. Electron.* **1** 127
[246] Dediu V, Murgia M, Matacotta F C, Taliani C and Barbanera S 2002 *Solid State Commun.* **122** 181
[247] Xiong Z H, Wu D, Valy Vardeny Z and Shi J 2004 *Nature* **427** 821
[248] Wohlgenannt M, Valy Vardeny Z, Shi J, Francis T L, Jiang X M, Mermer Ö, Veeraraghavan G, Wu D and Xiong Z H 2005 *IEE Proc. Circuits Devices Syst.* **152** 385
[249] Wang F J, Xiong Z H, Vu D, Shi J and Valy Vardeny Z 2005 *Synth. Met.* **155** 172-175
[250] Wu D, Xiong Z H, Li X J, Valy vardeny Z, Shi J 2005 *Phys. Rev. Lett.* **95** 016802
[251] Majumdar S, Laiho R, Laukkanen P, Väyrynrn I J, Majumdar H R and Österbacka R 2006 *Appl. Phys. Lett.* **89** 122114
[252] Kumar J, Singh R V, Siwach P K, Singh H K, Singh R, Rastogi R C and Srivastava O N 2006 *Solid State Commun.* **138** 422
[253] Santos T S, Lee J S, Migdal P, Lekshmi I C, Satpati B and Moodera J S 2007 *Phys. Rev. Lett.* **98** 016601
[254] Riminucci A, Bergenti I, Hueso L E, Murgia M, Taliani C, Zhan Y, Casoli F, de Jong M P and Dediu V 2007 *Preprint* cond-mat/0701603
[255] Lin B C, Cheng C P, You Z-Q and Hsu C-P 2005 *J. Am. Chem. Soc.* **127** 66
[256] Pramanik S, Bandyopadhyay S and Cahay M 2004 *Appl. Phys. Lett.* **84** 266
[257] Pramanik S, Bandyopadhyay S and Cahay M 2005 *IEEE Trans. Nanotechnol.* **4** 2
[258] Francis T L, Mermer Ö, Veeraraghavan G and Wohlgenannt M 2004 *New J. Phys.* **6** 185
[259] Mermer Ö, Veeraraghavan G, Francis T L and Wohlgenannt M 2005 *Solid State Commun.* **134** 631

[260] Sheng Y, Nguyen T, Veeraraghavan G, Mermer Ö, Wohlgenannt M, Qiu S and Scherf U 2006 *Phys. Rev.* B **74** 045213

[261] Wohlgenannt M 2006 *Preprint* cond-mat/0609592

[262] Ouyang M and Awschalom D D 2003 *Science* **301** 1074

[263] Pasupathy A N, Bialczak R C, Martinek J, Grose J E, Donev L A K, McEuen P L and Ralph D C 2004 *Science* **306** 86–9

[264] Goldhaber-Gordon D, Shtrikman H, Mahalu D, Abush-Magder D, Meirav U and Kastner M A 1998 *Nature* **391** 156

[265] van der Wiel W G, De Franceschi S, Fujisawa T, Elzerman J M, Tarucha S and Kouwenhoven L P 2000 *Science* **289** 2105

[266] Petta J R, Slater S K and Ralph D C 2004 *Phys. Rev. Lett.* **93** 136601

[267] Chen J, Reed M A, Rawlett A M and Tour J M 1999 *Science* **286** 1550

[268] Ralls K S, Buhrmann R A and Tiberio R C 1989 *Appl. Phys. Lett.* **55** 2459

[269] Bumm L A, Arnold J J, Dunbar T D, Allara D L and Weiss P S 1999 *J. Phys. Chem.* B **103** 8122

[270] Wold D J and Frisbie C D 2001 *J. Am. Chem. Soc.* **123** 5549

[271] Cui X D, Zarate X, Tomfohr J, Sankey O F, Primak A, Moore A L, Moore T A, Gust D, Harris G and Lindsay S M 2002 *Nanotechnology* **13** 5

[272] Wang W, Lee T and Reed M A 2003 *Phys. Rev.* B **68** 035416

[273] Liu R, Ke S, Baranger H U and Yang W 2005 *Nano Lett.* **5** 1959